Conformation and Affinity Modulations by Multiple Phosphorylation Occurring in the BIN1 SH3 Domain Binding Site of the Tau Protein Proline-Rich Region

Alessia Lasorsa, Krishnendu Bera, Idir Malki, Elian Dupré, François-Xavier Cantrelle, Hamida Merzougui, Davy Sinnaeve, Xavier Hanoulle, Jozef Hritz, Isabelle Landrieu

Conformation and affinity modulations by multiple phosphorylation occurring in the BIN1 SH3 domain binding site of Tau protein proline-rich region

Alessia Lasorsa[1,2 †#], Krishnendu Bera[3, 4, 5#], Idir Malki1[#], Elian Dupré[1,2], François-Xavier Cantrelle[1,2], Hamida Merzougui[1], Davy Sinnaeve[1,2], Xavier Hanoulle[1,2], Jozef Hritz[3, 5] and Isabelle Landrieu[1,2*]*

[1]CNRS EMR9002 Integrative Structural Biology, F-59000, Lille, France

[2]Univ. Lille, Inserm, CHU Lille, Institut Pasteur de Lille, U1167 - RID-AGE - Risk Factors and Molecular Determinants of Aging-Related Diseases, F-59000, Lille, France

[3]CEITEC MU, Masaryk University, Kamenice 753/5, 625 00 Brno, Czech Republic

[4]National Centre for Biomolecular Research, Faculty of Science, Masaryk University, Kamenice 5, 625 00, Brno, Czech Republic

[5]Department of Chemistry, Faculty of Science, Masaryk University, Kamenice 5, 625 00 Brno, Czech Republic

KEYWORDS protein-protein interactions, tau protein, phosphorylation, intrinsically disordered proteins, Alzheimer's disease, nuclear magnetic resonance spectroscopy, molecular dynamics

ABSTRACT

An increase in phosphorylation of the Tau protein is associated with Alzheimer's disease (AD) progression through unclear molecular mechanisms. In general, phosphorylation modifies the interaction of intrinsically disordered proteins, such as Tau, with other proteins, however elucidating the structural basis of this regulation mechanism remains challenging. The bridging integrator-1 gene is an AD genetic determinant whose gene product, BIN1, directly interacts with Tau. The proline-rich motif recognized within a Tau(210-240) peptide by the SH3 domain of BIN1 (BIN1 SH3) is defined as $_{216}$PTPP$_{219}$, and this interaction is modulated by phosphorylation. Phosphorylation of T217 within the Tau(210-240) peptide led to a 6-fold reduction in the affinity while single phosphorylation at either T212, T231 or S235 had no effect on the interaction. Nonetheless, combined phosphorylation of T231 and S235 led to a 3-fold reduction in the affinity, although these phosphorylations are not within the BIN1 SH3-bound region of the Tau peptide. Using nuclear magnetic resonance (NMR) spectroscopy, these phosphorylations were shown to affect the local secondary structure and dynamics of the Tau(210-240) peptide. Models of the (un)phosphorylated peptides were obtained from molecular dynamics (MD) simulation validated by experimental data, and showed compaction of the phosphorylated peptide due to increased salt bridge formation. This dynamic folding might indirectly impact the BIN1 SH3 binding by a decreased accessibility of the binding site. Regulation of the binding might thus not only be due to local electrostatic or steric effects from phosphorylation, but also to the modification of the conformational properties of Tau.

INTRODUCTION

Post-translational modifications (PTMs) in general, and most notably phosphorylation, play a major role in regulating protein functions, and in particular those of intrinsically disordered proteins (IDPs). IDPs do not fold into a stable three-dimensional structure but exist in dynamic equilibrium between different conformations. IDPs are solvent exposed and thus susceptible to multiple modifications that modulate their properties.[1–3] Phosphorylation, namely the attachment of a phosphate group to specific amino acid side chains, not only increases the steric hindrance, but also results in the addition of negative charges (1.5 - 2 negative charges per amino acid at pH 6.5 - 7.5), accounting for new electrostatic properties of the modified protein. These extra charges can directly interfere with the molecular interaction network through electrostatic effects, but can also exert an indirect effect by modulating the local and global conformations of the IDPs.[4,5] Phosphorylation can (de)stabilize transient secondary structural elements in IDPs, leading to disorder-to-order transitions[6,7] and perturbation of the ensemble of conformations.[8] In addition, the multiple phosphorylations interplay in a complex manner, which can lead to a linear response described as a "rheostat" [9] or an ultrasensitive response involving a threshold.[6,10]

The neuronal Tau protein is a prime example of an IDP with its functions regulated by phosphorylation. The longest isoform of Tau has 441 amino acid residues with 80 potential phosphorylation sites, of which 55 are confirmed by mass spectrometry analysis.[11] Tau phosphorylation is of particular interest because Tau is found hyperphosphorylated in Alzheimer's disease (AD). These multiple serine/threonine sites combine into different profiles of phosphorylation as they can be targeted by various kinases, each of them with its own specificity for a subset of the serine/threonine residues. Each specific phosphorylation combination potentially affects Tau functional properties in a different manner. For example, 3 phosphorylation

sites out of the four pS202 (phospho-serine 202)/pT205 (phospho-threonine 205) and pT231/pS235 are necessary to abolish the tubulin polymerization capacity of Tau, whereas 2 phosphorylations, either pS202/pT205 or pT231/pS235, have no effect on Tau function of tubulin polymerization.[12] Phosphorylation of Tau at these sites was shown to stabilize secondary structural elements, including a short helix for pT231/pS235[13,14] and a dynamic turn conformation for pS202/pT205.[15] Multiple phosphorylation of Tau were also proposed to affect Tau transient folding,[16] described as a paperclip.[17,18] The impact of Tau phosphorylation on its molecular interactions therefore cannot be reduced to the direct electrostatic and steric effects, but also involves its local and global conformations. However, establishing a direct link between PTMs, interaction and conformation in IDPs remains a challenging task.

The bridging integrator 1 gene (*BIN1*) is a major genetic risk factor for AD, and the SH3 domain of the BIN1 protein (BIN1 SH3) interacts directly with the Tau proline-rich region.[19,20] Molecular details of this interaction have previously been described.[21,22] The Tau(210-240) peptide fully encompasses the interaction site, is enriched in charged residues and contains 8 proline residues. The proline-rich motif PPII.2 (216-221) of Tau is bound to the Pro-binding pocket of BIN1 SH3 domain while the region downstream this binding site, up to Tau V229, is in interaction with the negatively-charged specificity surface of BIN1 SH3. Phosphorylation of Tau in the proline rich region was shown to reduce the interaction with BIN1 protein, and phosphorylated Tau(210-240) peptide exhibits a decreased affinity for BIN1 SH3.[20,22] These data were used in order to rationalize on a molecular basis the effect of specific phosphorylation, located directly in the binding site or at distal positions within Tau(210-240) peptide, on the binding affinity to BIN1 SH3. The effect of such PTMs on the secondary structure of Tau peptides, were first investigated by nuclear magnetic resonance spectroscopy (NMR) to better understand the parameters that can affect the

interaction due to multiple phosphorylation. In addition, models obtained from molecular dynamics (MD) simulations provided insights on the preferential fold of the Tau(210-240) peptide. Our data indicated that multiple phosphorylation induced the formation of transient secondary motifs and modification of the global fold of the peptide, which became more compact and less flexible. All these property modifications could conspire to affect the binding properties of the phosphorylated Tau peptide.

METHODS

Proteins and peptides BIN1 SH3 domain and Tau(210-240) peptide SRTPSLPTPPTREPKKVAVVRTPPKSPSSAK were produced in *Escherichia coli* fused to an N-terminal histidine-tag or a histidine-tagged SUMO domain, respectively, as previously described.[21] Uniformly labeled ^{15}N and ^{13}C or ^{15}N protein/peptide samples were produced in M9 medium containing 0.1% $^{15}NH_4Cl$ and 0.2% ^{13}C-glucose (Sigma-Aldrich) or 0.4% ^{12}C-glucose, supplemented with 0.5 g/l of ^{15}N-enriched and ^{13}C-enriched or ^{15}N-enriched ISOGRO (Sigma-Aldrich), depending on the labeling scheme, 0.1 mM $CaCl_2$ and 2 mM $MgSO_4$. Unlabeled Tau(210-240) phosphopeptides for dissociation constant determination were prepared by solid phase synthesis (Genecust, France) - except for the 4P-Tau(210-240) peptide sample, which was enzymatically phosphorylated. After resin cleavage, peptides were purified by reverse-phase high-performance liquid chromatography. The purity of the phosphopeptides were >95%. The molecular weight of each peptide was confirmed by mass spectrometry.

Enzymatic phosphorylation Phosphorylation of His6-SUMO-Tau(210-240) was obtained by incubation with recombinant CDK2/CycA3 kinase,[23] at a molar ratio of 1/100, as described.[22] Phosphorylated His6-SUMO-Tau(210-240) was next incubated for 16 h with SENP2 protease in the presence of 2 mM DTT, at 4°C, in order to cleave the His6-SUMO tag. A nickel affinity

chromatography step was performed immediately after cleavage to remove the His6-SUMO tag. The phosphorylated Tau(210-240) peptide (a mixture of 3P-Tau(210-240) and 4P-Tau(210-240)) was buffer-exchanged using a desalting column (G25 resin, cutoff of 7 kDa; PD-10 Cytiva) against 50 mM sodium phosphate pH 7.3, 30 mM NaCl and 3 mM DTT. A cation-exchange chromatography step was next necessary to remove the 3P-Tau(210-240) (phosphorylation at T212, T231 and S235) to obtain an homogeneous 4P-Tau(210-240) peptide (phosphorylation at T212, T217, T231 and S235) (**Figure S1**). The cation exchange resin (Mono S HR 5/5 GE Healthcare) was equilibrated with 50 mM ammonium acetate, pH 4.6. The sample load was typically 5 mL, 200 µM. Elution was achieved with a linear gradient of NaCl. Phosphorylation at T212, T217, T231 and S235 was assessed by mass spectrometry analysis.

NMR spectroscopy NMR experiments were recorded on an AVANCE NEO Bruker 900 MHz or AVANCE I 600-MHz spectrometers both equipped with a triple-resonance cryogenic probe. NMR measurements to characterize Tau peptides were performed in 50 mM phosphate buffer, pH 6.5, 30 mM NaCl, 3 mM DTT and 10% (v/v) D_2O (NMR buffer), at 278 K to reduce amide proton-solvent exchange. Tau(210-240) and 4P-Tau(210-240) backbone and side-chain assignments at 278 K have been reported.[22] 3D NOESY peak lists for both Tau(210-240) and 4P-Tau(210-240) were extracted from ^{15}N- and ^{13}C-edited spectra. ^{15}N-R1, ^{15}N-R2, and ^{15}N steady-state heteronuclear NOE (hetNOE) spectra were recorded at 278 K on ^{15}N-labeled Tau peptide samples (0.12 mM) at 600MHz. For the R1 experiments, 11 data points were recorded, using relaxation delays between 50 and 1300 ms and a recycle delay of 4 s. For R2 experiments, 13 data points were recorded, using relaxation delays between 10 and 150 ms (recycle delay was 4 s). The hetNOE experiment was recorded by including, or not, a 5 s period of 120° ^{1}H saturation pulses, separated by 5 ms. Recovery delay was 4 s. Uncertainties in peak intensities for ^{15}N-R1 and ^{15}N-

R2 were estimated from two non-successive duplicate data points: 0.6 s for R1 and 40.8 ms for R2 experiments, respectively. Uncertainties in peak intensities for hetNOE were estimated from the signal to noise ratio of each resonance. 3D HN-HA spectra were recorded at 278 K on ^{15}N-labeled Tau peptide samples (0.3 mM) at 600 MHz. A direct measure for the magnitude of $^{3}J_{HN\text{-}H\alpha}$ was provided by the intensity ratio between the cross-peaks at (F1,F2,F3)=(N,HA,NH) and the diagonal peaks at (F1,F2,F3)=(N,NH,NH).

NMR data analysis Spectra were processed using TopSpin software (Bruker) and analyzed by CcpNmr Analysis[24] and NMRPipe.[25] Two analysis were performed to evaluate the secondary structure preference of Tau(210-240) peptides. Firstly, the delta2D method uses Hα, Cα, Cβ, CO, N and HN chemical shift values with only the first and the last residue excluded from the analysis.[26] The percentage of occupancy of a secondary structure element is obtained by comparing the experimental chemical shifts with values from a reference database of high-resolution native state conformations from which chemical shift measurements are available. Secondly, secondary chemical shifts (^{13}Cα-^{13}Cβ differences) were used as indicators for residual local secondary structure by calculating the deviation from neighbour-corrected random coil chemical shift values.[27] For the phosphorylated residues, the reference values for serine and threonine residues were replaced with random coil values for phospho-serine and phospho-threonine.[28,29]

Dissociation constant determination Titration of 70 µM ^{15}N-BIN1 SH3 with increasing amount of unlabeled Tau(210-240) peptides (from 35 µM to 840 µM) was performed in 50 mM phosphate buffer pH 7.3, 30 mM NaCl by monitoring the complex formation using the gradual ^{1}H and ^{15}N chemical shift change of the resonances in ^{1}H,^{15}N HSQC, at 293 K (**Figure S2**). The weighted average chemical shift differences were calculated as described by Garrett et al.[30] - i.e. $((\Delta H^2 + (\Delta N/5)^2)/2)^{1/2}$, with ΔH and ΔN the chemical shift changes for ^{1}H and ^{15}N,

respectively. Dissociation constants were obtained by fitting the chemical shift perturbation data to the following equation: $\Delta\delta_{obs} = \Delta\delta max((a+b+K_d-((a+b+K_d)^2-4ab)^{1/2})/2a)$ where $\Delta\delta_{obs}$ is the observed chemical shift perturbation (including both proton and ^{15}N nuclei) and $\Delta\delta max$ is the maximal signal change upon saturation. K_d is the dissociation constant, and a and b are the peptide and BIN1 SH3 total concentrations, respectively. Dissociation constants K_d were averaged, and standard deviations provided, based on chemical shift perturbation analysis of 10 distinct resonances.

MD simulations Tau(210-240) peptide was modelled keeping all prolines in *trans* conformation. Phosphorylation sites were inserted at T212, T217, T231 and S235 using the PyTMs plugin[31] of PyMOL.[32] MD simulations were performed at 278 K, 298 K and 310 K, using GROMACS 5.1.4 package[33] with the Amber99SB-ILDN (A99)[34] or CHARMM36m (C36m)[35] force fields for the protein atoms and TIP4P-D[36] for the water molecules (**Table S1**). The choice of force fields and water model was based on Zapletal *et al.* 2020.[37] Details of the performed simulations can be found in **Table S1**. The charge of the phosphorylated threonine and serine residues was set as -2e and the end terminals were capped with NH_3^+ and COO^- groups. The peptides were solvated using cubic boxes where the protein was inserted at the centre and at a minimal distance of 2 nm from the box edges. Periodic boundary conditions were employed and the bond length along with hydrogen atoms were constrained using LINCS algorithm.[38,39] The short range electrostatics and the Lennard-Jones interactions were cut-off at 1.0 nm. The long-range electrostatics were calculated using particle mesh Ewald (PME) summation with 0.12 nm grid spacing. The charge of the system was neutralized by adding sodium and chloride ions and the concentration of salt was adjusted to 50 mM to mimic the experimental ionic strength. The systems were energy minimized using the steepest descent algorithm followed by series of

equilibrations for 100 ps NVT to heat up the systems to reach the desired temperature (278 K, 298 K and 310 K) while restraining protein position at 1000 kJ mol^1 nm^2 for relaxation of water molecules and backbone atoms (1000 kJ mol^1 nm^2) using V-scale temperature coupling[40] with a coupling constant (τT) of 0.1 ps. Further 500 ps backbone atoms restrained (1000 kJ mol^1 nm^2) and unrestrained 1 ns NPT steps were performed using Parrinello-Rehman barostat[41] with a coupling constant (τP) of 2 ps and 1 bar pressure. Other parameters were kept similar as per our previous MD simulation studies.[37,42] Finally, 1 μs production simulations were performed for each system with a 2 fs time step. Based on the initial results C36m systems were further prolonged for another 1 μs each. From all MD trajectories, we calculated the $^3J_{HN\text{-}H\alpha}$ couplings using Karplus equation with the Karplus constants set to A = 6.51, B = -1.76 and C = 1.6, using gmx chi program.[33] Chemical shifts were calculated using SHIFTX2 for each snapshot from the trajectories[43] and the C_α-C_β secondary chemical shift (Δδ) values were calculated by subtracting the random-coil values.[27] The other analyses were performed using in-house scripts, GROMACS inbuilt analysis tools[33] and contact maps were calculated using CONAN.[44]

RESULTS

Phosphorylation at T212/T217/T231/S235 modulates the interaction of Tau with BIN1 SH3

The effect of Tau phosphorylation at specific sites on BIN1 SH3/Tau interaction was investigated with a series of Tau(210-240) peptides phosphorylated at specific threonine or serine residues. The dissociation constants Kd of the interaction with the BIN1 SH3 domain were measured by NMR (**Figure 1A-C**). Increasing amounts of unlabeled peptides were added to ^{15}N-labeled BIN1 SH3 domain and the titration was followed by recording ^{1}H,^{15}N HSQC NMR spectra (**Figure S2**). The Kd of the BIN1 SH3/Tau(210-240) interaction was found to be 44 ± 3 μM. Phosphorylation at T217, directly in the proline-rich binding motif of Tau corresponding to a PPII.2 proline-rich motif

(216-221),[22] showed a 6-fold reduction in affinity (Kd = 283 ± 46 μM). In contrast, phosphorylation at T212 had no effect on the binding (same Kd as Tau(210-240)). In accordance, for a double phosphorylation pT212pT217, a Kd value of 280 ± 28 μM was found, further indicating no contribution of T212 to the interaction. Single phosphorylation at T231 or S235 did not affect the binding affinity (Kd = 38 ± 10 μM). However, simultaneous phosphorylation at these two sites showed an unexpected 3-fold reduction in the affinity (Kd = 123 ± 7 μM). There was no obvious molecular basis for the observed weaker interaction due to such combined phosphorylations because these residues - T231 or S235 - showed no contacts with the BIN1 SH3 domain (**Figure 1D**).[22] Kd measurements performed with a tetraphosphorylated 4P-Tau(210-240) peptide, pT212pT217pT231pS235 pattern, showed a Kd value of 575 ± 126 μM. The phosphorylation on four sites was expected to have no more impact on the interaction than pT217 alone (Kd = 283 ± 46 μM), because the other three phosphorylations pT212, pT231 or pS235 had no effect individually. This Kd value thus indicates a non-linear response compared to the Kd values measured for each mono-phosphorylated peptide.[45] Although the affinity of the phosphorylated peptides was decreased, they conserved the same binding mode to BIN1-SH3 compared to Tau(210-240) (**Figure S3**). This led us to consider that phosphorylation could modulate the interaction by both direct electrostatic repulsive effects and indirect conformational changes of the Tau peptide due to combined phosphorylations.

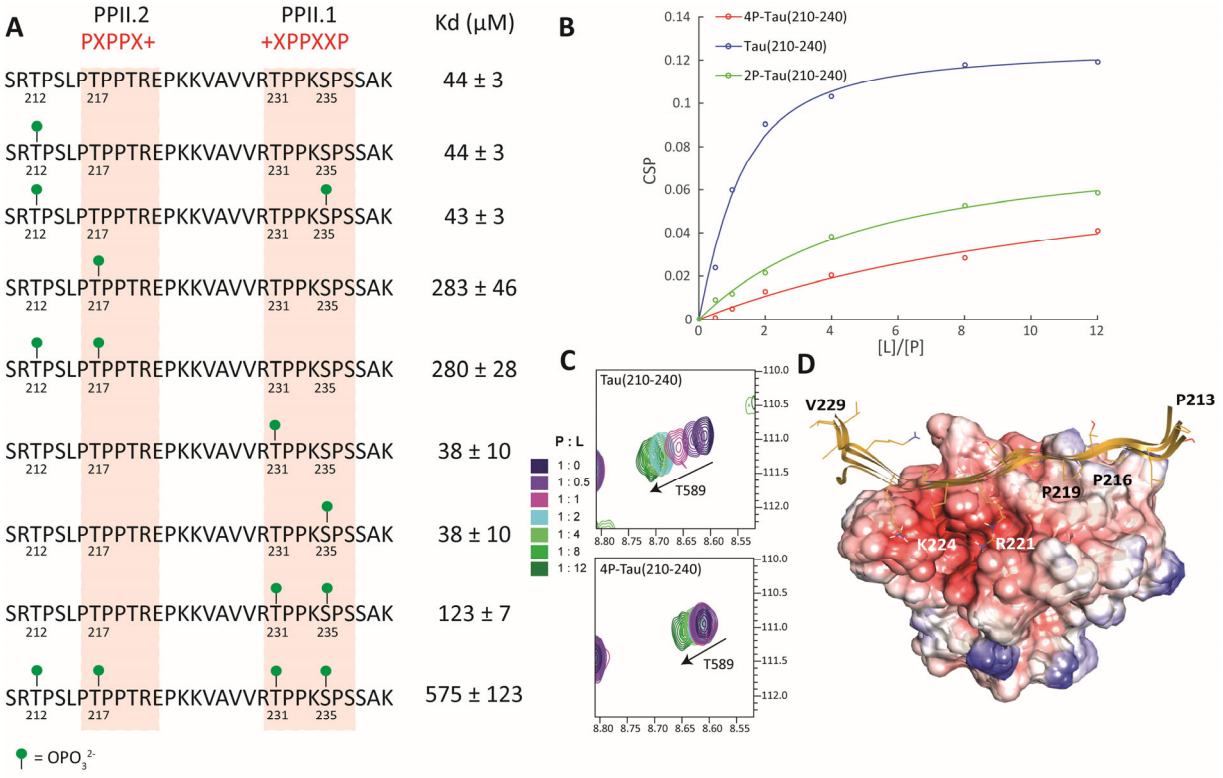

Figure 1. Interaction of BIN1 SH3 with Tau peptides. **A.** Dissociation constant (Kd) values of different phosphorylated Tau(210-240) peptides binding to BIN1 SH3, determined by NMR titration experiments. **B.** Chemical shift perturbation values of the $^{1}H,^{15}N$ resonance of T589 residue of BIN1 SH3 (P = 70 µM) versus increasing amounts of Tau(210–240) (L, from 35µM to 840 µM, blue curve), 2P-Tau(210–240) (green curve, pT212/pT217) and 4P-Tau(210–240) (red curve). Dots represent experimental values, while the curve is obtained from the fitted saturation equation. **C.** Superposition of $^{1}H,^{15}N$ HSQC spectra of BIN1 SH3 (P) zoomed around T589 resonance in the presence of increasing amounts of Tau(210–240) or 4P-Tau(210–240) (L) (from blue to green) (c). **D.** Accessible surface representation of BIN1 SH3 (color according to the electrostatic potential, from red-negative to blue-positive) in complex with Tau (213–229) peptide (ribbon representation in gold). Side-chains are represented as sticks.

Impact of phosphorylation on Tau(210-240) secondary structure propensity The effects of phosphorylation on local conformation were thus next investigated by NMR by using the backbone and side-chain (Hβ, Cβ) chemical shift values of Tau(210-240) and 4P-Tau(210-240) peptides (**Figure 2A-C**), which are influenced by the backbone dihedral angles. We first extracted local secondary structure preferences using the delta2D method,[26] which provides a global view of the modification upon phosphorylation by use of Hα, Cα, Cβ, CO, N and HN chemical shift values. We found an increase in the β-strand propensity for the 4P-Tau(210-240) peptide, between residues L215-P219 and R230-K234, coupled with a decrease in the random coil and PPII content (**Figure 2D**). A small increase in the α-helical propensity was also observed at the C-terminus of the peptide. Additional direct analysis of Cα and Cβ chemical shifts relative to random coil values[28,29] showed that phosphorylation indeed increased the α-helical propensity at residues P236–A239 (**Figure 2E**), which are located downstream of the pT231/pS235 phosphorylation sites (**Figure 1A**). Increased α-helical propensity was also observed at the N-terminus, most likely due to phosphorylation at residue T212. Performing an analogous characterization on a Tau mutant peptide (T231A), with only T212 and S235 phosphorylated (same affinity to BIN1 SH3 as Tau(201-240)), we observed a decrease in the α-helical content at the C-terminus, compared to a 4P-Tau(210-240) peptide with both pT231 and pS235 (**Figure 2E**). This showed that pT231 contributed to strengthen the α-helical content at the C-terminus, but it was not essential.

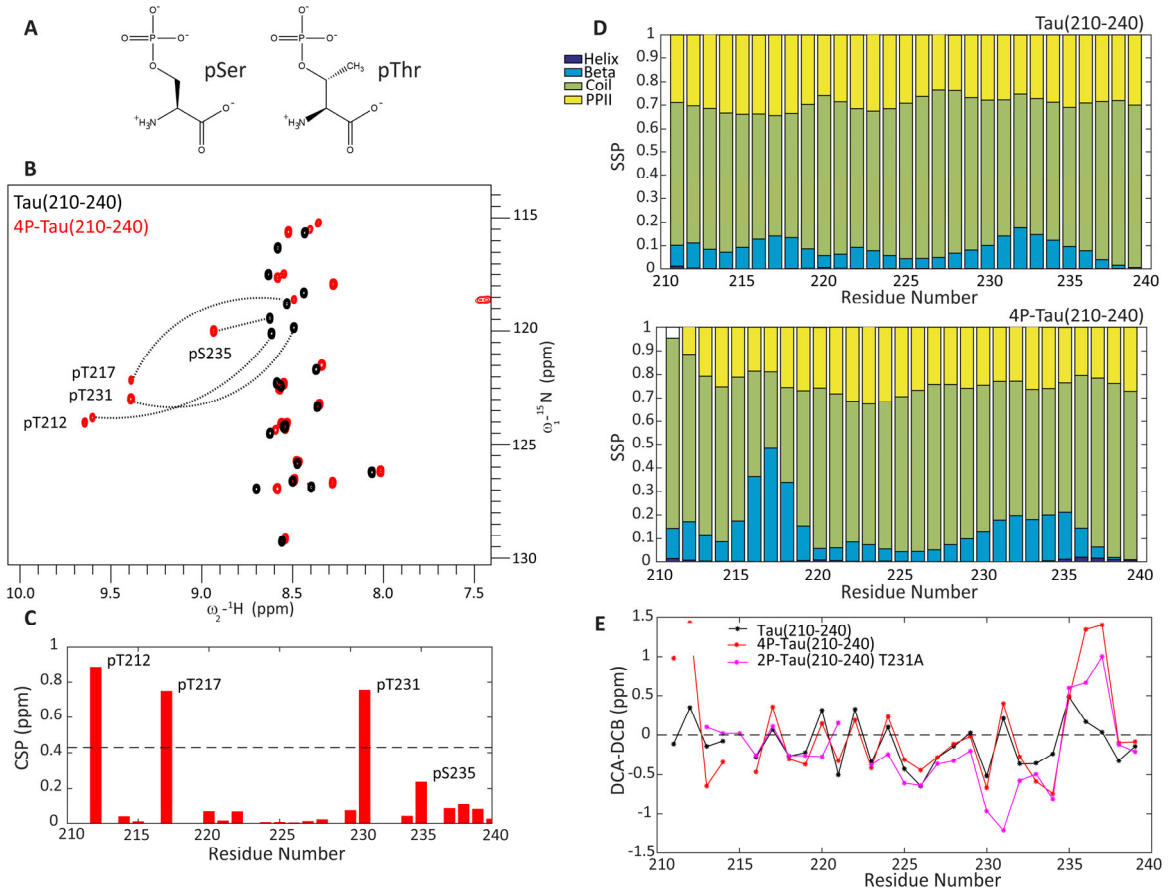

Figure 2. Secondary structures of the Tau peptides. A. Molecular structures of phosphorylated serine and threonine. B. Overlay of ^{1}H,^{15}N HSQC spectra of Tau(210-240) and 4P-phosphorylated Tau(210-240) C. Chemical shift perturbation (CSP) plot, units are in ppm. D. Delta2D analysis based on Hα, Cα, Cβ, CO, N and HN chemical shifts for Tau(210-240) (above) and 4P-Tau(210-240) (below) that gives the relative abundance or secondary structure propensity (SSP) for each of the secondary structures, polyproline II helix, β-strand and α-helix or coil conformation along the peptide sequence. E. Secondary chemical shifts calculated using Cα and Cβ chemical shift value differences. Positive values represent preferential α-structure and negative values β-structure preferences.

$^{3}J_{HN\text{-}H\alpha}$ values correlate with the Φ backbone dihedral angles of the N-Cα bonds and are thus indicative of secondary structure preferences. $^{3}J_{HN\text{-}H\alpha}$ values between 6 and 8 Hz are typical for disordered conformations. Significantly lower values (3-4 Hz) were observed for the phosphorylated threonine residues (**Figure 3**), indicating a higher propensity for more ordered compact conformations, as it has been previously reported.[46,47]Analysis of 3D NOESY spectra of the Tau peptides showed mainly sequential NOE contacts between HN of residue i and Hα/Hβ of residue i-1, typical of disordered conformations (**Figure S4**, **Tables S2-3**). However, in the case of the 4P-Tau(210-240) peptide, additional sequential NOEs were observed between pT231 HN and R230 HN, and between several HN (i) and Hβ (i-1) of residues located within the P233-A239 sequence (**Figure S4B**). In addition, two non-sequential NOEs pT231 HN-V229 Hγ and pT231 HN-A227 Hβ demonstrated the compaction of the C-terminal part of the phosphorylated peptide. These NOE signals indicative of spatial proximities concurred with J-coupling and secondary chemical shift analysis to report a more ordered conformation for the phosphorylated peptide.

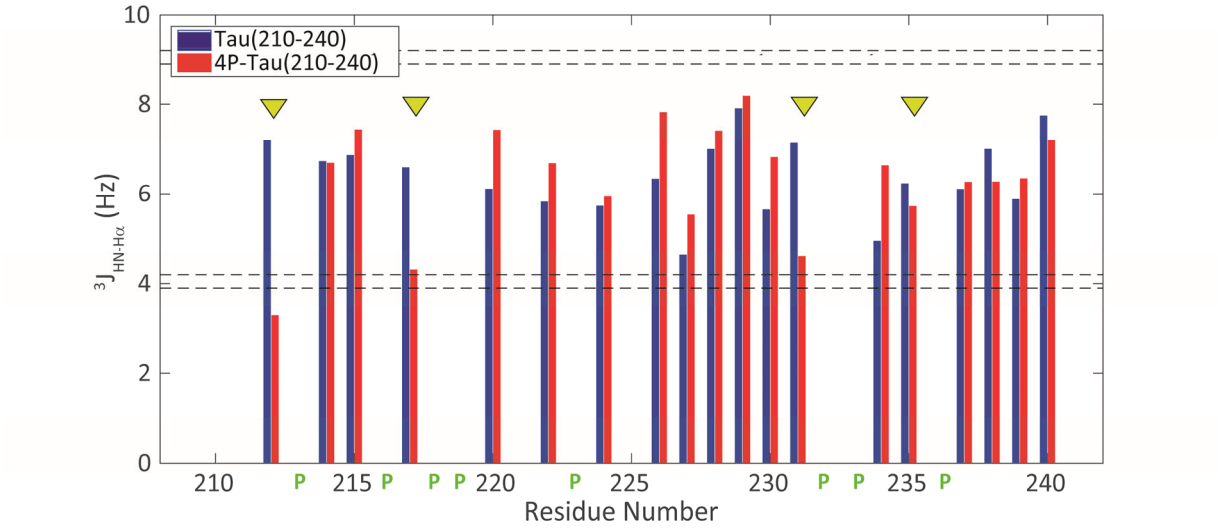

Figure 3. Analysis of coupling constants. ^{3}JHN-Hα couplings for Tau(210-240) and 4P-Tau(210-240). Horizontal lines are marked at 3.9, 4.2, 8.9 and 9.2 Hz, representative values for α-helix, 3^{10}-

helix, parallel β-sheet and antiparallel β-sheet, respectively. Proline residue positions in the sequence are indicated by a green P along the x-axis.

Impact of phosphorylation on Tau(210-240) backbone dynamic parameters To define whether these conformational modifications due to phosphorylation could affect the peptide dynamics properties, we used NMR relaxation parameters as reporters.[48] Thus, we measured longitudinal relaxation rates (R_1), transverse relaxation rates (R_2), and steady-state $^{1}H,^{15}N$ heteronuclear NOE (hetNOE) values, for both Tau(210-240) and 4P-Tau(210-240) peptides, to probe the impact of phosphorylation on Tau(220-240) peptide dynamics (**Figure 4**).

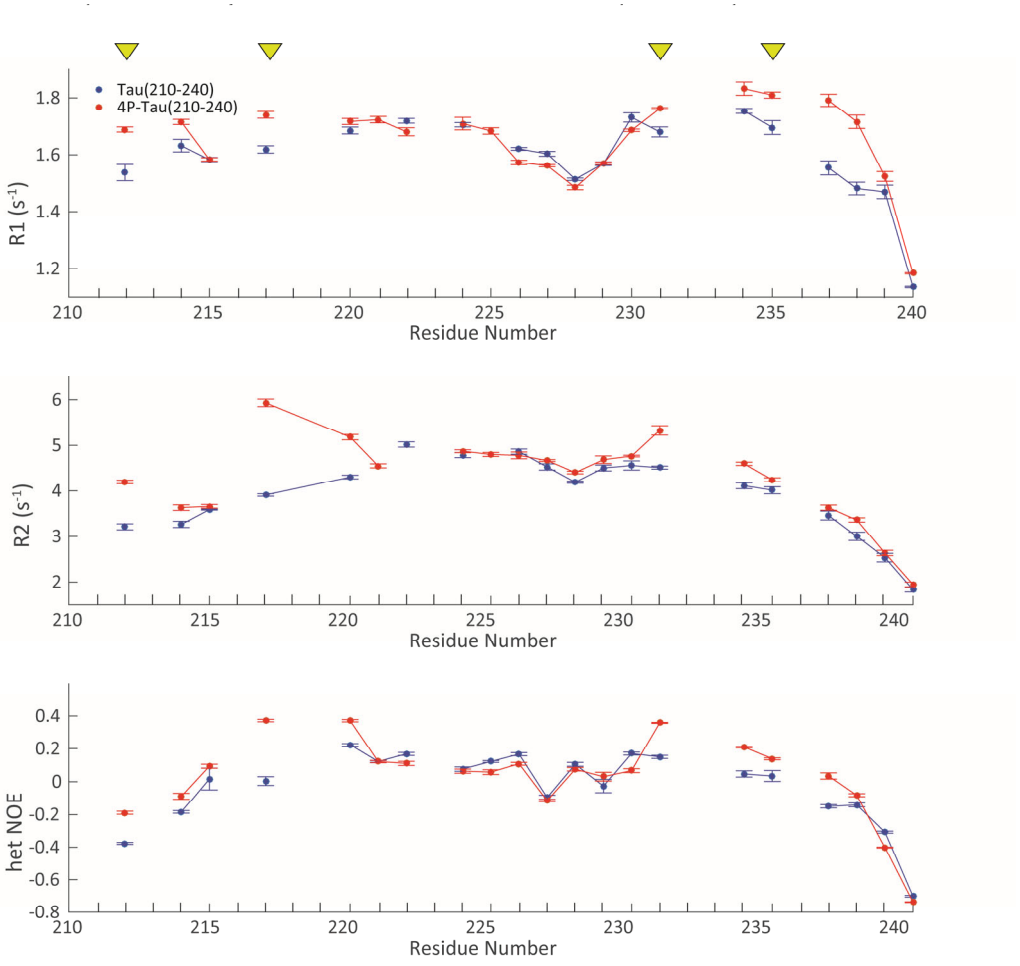

Figure 4. Dynamics of Tau peptides. Relaxation rates R1, R2 and $^{1}H,^{15}N$ heteronuclear NOE (hetNOE) of Tau(210-240) and 4P-Tau(210-240). Arrow heads indicate the phosphorylation sites.

The R_1, R_2, and hetNOE measurements are sensitive to motions on the nanosecond to picosecond timescales, whereas R_2 relaxation rates are additionally influenced by dynamics on the millisecond to microsecond timescales. An increase in R_1, R_2 and hetNOE was observed for the pT residues, suggesting a reduction in internal motions. An increase in R1 and hetNOE was also observed for the sequence 234-238 at the C-terminus, in agreement with a decrease in the flexibility.

Molecular Dynamic simulations of Tau(210-240) conformation ensemble In order to characterize the tertiary structural properties of the Tau peptide, we performed calculations by using microsecond time-scale MD simulation. We first explored different simulation conditions **(Table S1)**, including two force fields (C36m and A99) and three temperatures (278 K, 298 K and 310 K). The full convergence was not obtained for all systems, even though the Tau peptide systems have been simulated in microseconds timescale. Nevertheless, the best simulation strategy was then chosen based on the agreement between experimental J couplings and secondary chemical shifts with values predicted from the generated structural ensembles (**Figure 5**).

The averaged root-mean-square deviation (RMSD) values between predicted and experimental secondary chemical shift and $^{3}J_{HN\text{-}H\alpha}$ coupling values showed that the C36m force field driven MD simulations produced the most reliable structural ensemble (**Figure 5, Figures S5 and S6**). Therefore, we used the C36m, at all three temperatures, in combination with TIP4P-D water model simulations to analyze the Tau peptide structural ensembles.

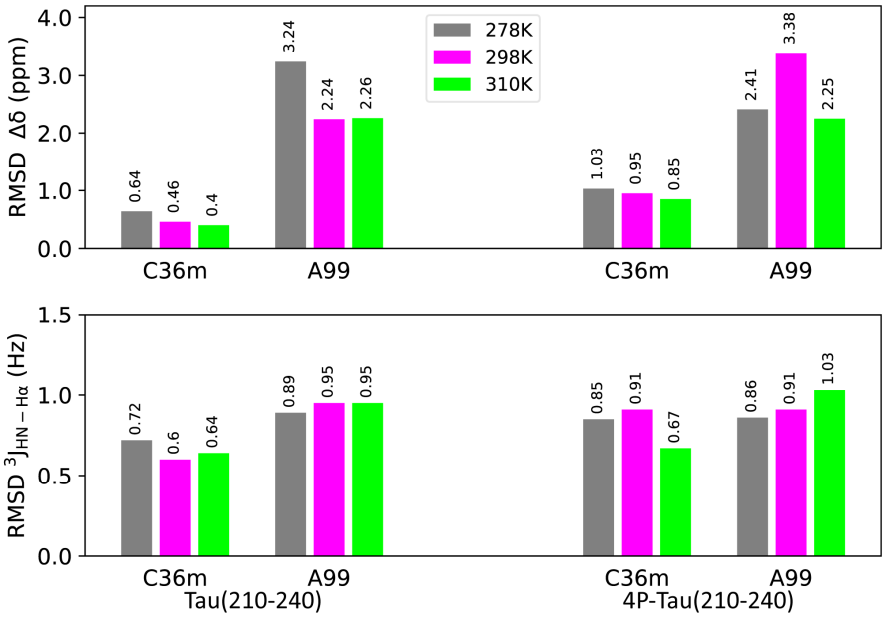

Figure 5. Validation of the MD simulations. RMSD of secondary chemical shift and $^{3}J_{HN\text{-}H\alpha}$ coupling values calculated from NMR experimental parameters and predicted from MD simulation trajectories.

Structural analysis of the MD-generated structural ensembles of Tau peptides To get a more detailed picture of the secondary structural preferences of Tau(210–240), we calculated the secondary structure propensity (SSP) scores for each residue using the DSSP tool (hydrogen bond estimation algorithm) (**Figure S7**).[49,50] The random coil state was the dominant conformation for every peptide ensemble, with a population of 75-88%. Upon phosphorylation, an increase in secondary structural elements was observed, defined as β-turn and β-bend conformations that are non-regular secondary structures that cause a change of direction of the backbone chain (**Figure S7**). To gain further insight into the characteristics of the chain folding, we calculated the time-dependent variation of the radius of gyration (R_g) **(Figure 6)**.

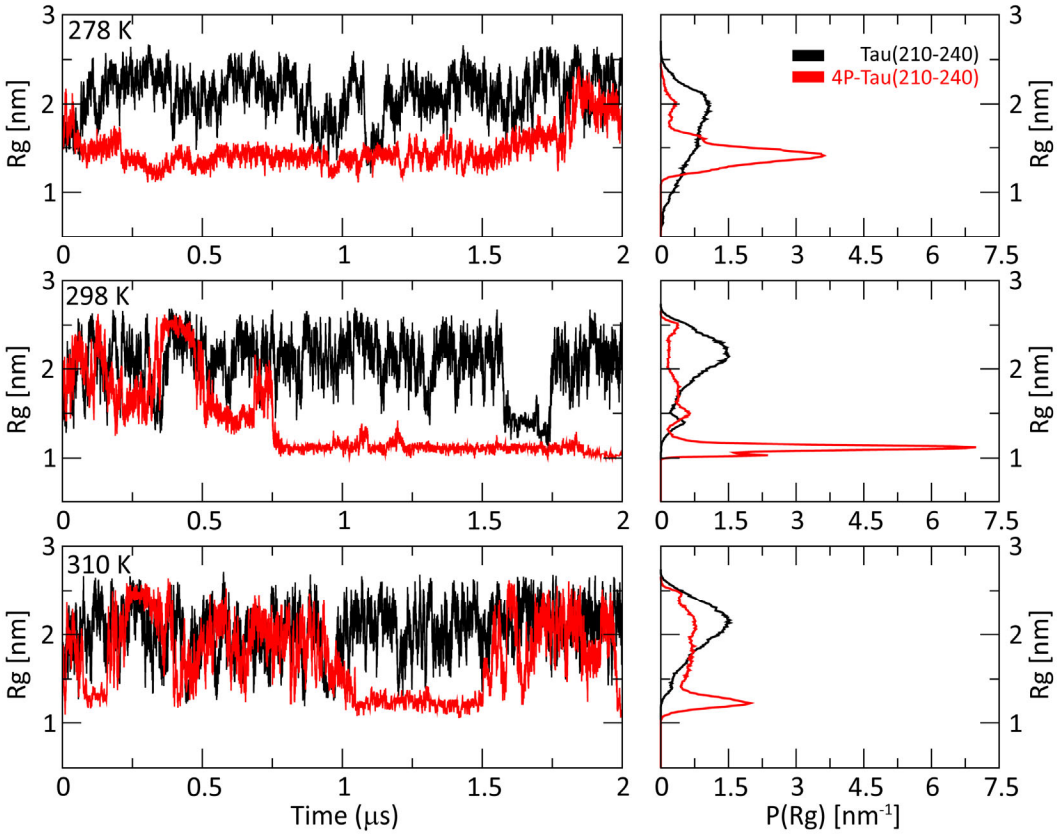

Figure 6. Preferential conformations of Tau peptides. Time dependent radius of gyration (Rg) along with its normalized distributions, from top to bottom at 278 K, 298 K and 310 K. Black curves represent Tau(210-240) and red curves 4P-Tau(210-240).

For the phosphorylated peptide, we observed a decrease of the average R_g values compared to Tau(210-240) specially at lower temperatures (**Table S4**). Contact maps (**Figures 7a**) for the structural ensembles generated by the C36m force-field showed indeed more contacts for the phosphorylated peptide with respect to the Tau(210-240) that is in an extended conformation. Most of the observed contacts originated from the pT217, pT231, pS235 phosphorylated residues (**Figures 7a**) that engaged in intramolecular salt bridges. (**Figures 7b and Table S5**).

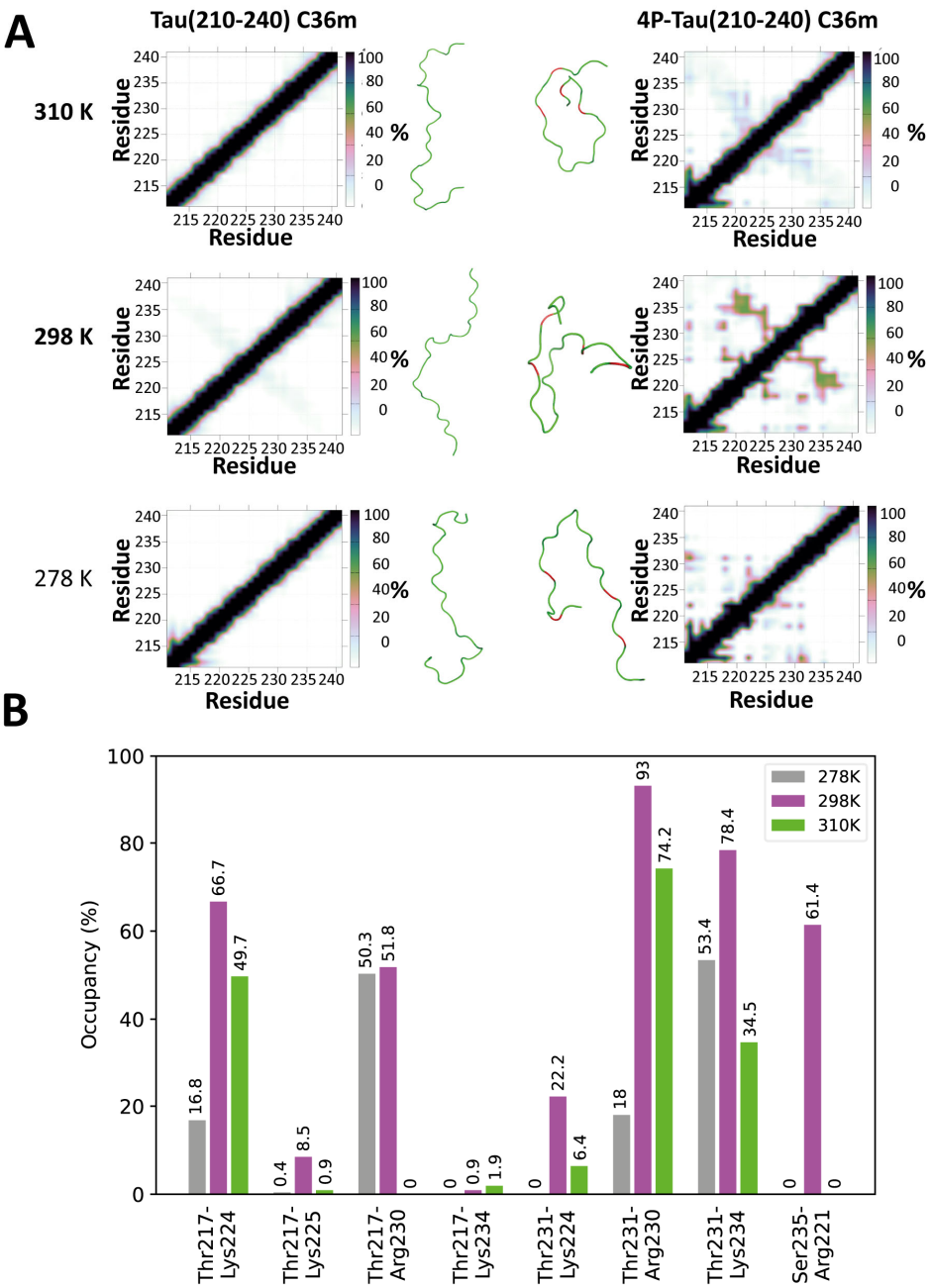

Figure 7. Intramolecular contacts of Tau peptides. **A**. Average contact maps describing the distances between residue pairs of Tau peptide simulated using C36m. The scales shown at the right indicate color coding of populations of events when the distance between any pair of residue atoms was shorter than 0.6 nm. A representative structure of Tau peptide is shown corresponding

to the final time point (2 μs) of the C36m force-field driven simulation with red colour showing the phosphorylated residues. **B.** Occupancy (%) of salt bridges for Tau(210-240) and 4P-Tau(210-240) peptides simulated by C36m force-field parameters.

DISCUSSION

Formation of a binding interface is governed by various determinants that will control the binding affinity. Even non-interfacial charges can have an effect on the strength of intermolecular interactions, affecting the kinetics of binding (Kon) and Kd.[51,52] Intrinsically disordered proteins differ from globular proteins in the kinetics of the binding process and the interactions stabilizing their complexes due to their specific sequence features.[5,53,54] Even more complex is the contribution of multiple phosphorylation to the regulation of their protein interactions. The impact of different phosphorylation patterns in the Tau(210-240) peptide on its interaction with BIN1 SH3 was not straightforward to rationalize based on local steric or electrostatic contributions to the binding surface alone. A similar observation was made for a polyproline sequence of the retinoic acid hormone nuclear receptor RARγ bound by the Vinexin β SH3 domain.[55] Introduction of a fluoroproline residue outside the canonical SH3–PPII binding motif of the RARγ polyproline peptide decreases the interaction, with a two-fold increase in the dissociation constant, although the fluorine atoms are not expected to contribute significantly to the protein–peptide binding interface. The effect is attributed to subtle conformational changes induced by the fluorination. In addition, within the Tau peptide, the multiple phosphorylation behave in a non-additive manner in regard to their single negative contribution to the binding. Phosphorylation of T231 and S235, located outside of the binding site negatively influenced the binding, but only when combined. Phosphorylation could thus indirectly influence the binding by modulating the structural parameters of the unbound Tau. We indeed observed that the phosphorylation affected the

secondary structure of Tau(210-240) peptide as well as its preferential conformation. Previous studies also indicate that phosphorylation in Tau proline-rich region induces structural changes of the protein backbone. NMR spectroscopy and CD analysis of phosphorylated Tau peptides (including Tau 211-238 with 6 phosphorylations) show that phosphorylation within these peptides leads to more compact and more ordered states. The strong decrease in the J coupling constant of the pT residues is observed specifically in the di-anionic states (pH 8.0).[46] However, reports on the impact of Tau phosphorylation in the proline rich region on the secondary structure propensity is not consensual and might be dependent on the sequence surrounding the phosphorylation site. Decreased coupling constant values for pT (**Figure 3**) were reported to indicate a decrease in the PPII population coupled to an increase in the β-strand population, in agreement with our observations (**Figure 2D**).[47] However, phosphorylation of the proline rich region of Tau promoting polyproline helix (PPII) was also reported, for pS and pT[46,56] or for pS alone, while pT alone has an opposite effect.[47] Similarly to our observations, an increased helical propensity at residues A239-R242 at the C-terminus of the pT231/pS235 sites has been reported,[13,57] with an additive effect due to further phosphorylation of S237 and S238.[14]

A decrease in the PPII helix propensity in the proline-rich binding motif might contribute to the decrease in the affinity for BIN1 SH3 once T217 is phosphorylated. This motif is well-known to adopt a PPII conformation in the SH3-bound state, and the presence of the bound-conformation in the free-state might favour the interaction.[58,59] Stabilization of the helical conformation at the C-terminus of 4P-Tau(210-240) is instead unlikely to impact the binding because a peptide with pT212 and pS235, with the same affinity for BIN1 SH3 as the unphosphorylated peptide (**Figure 1A**), still retains some higher helical content at the C-terminus compared to the unphosphorylated peptide (**Figure 2D**). Therefore, the decrease in the binding affinity for a combined

phosphorylation (pT231 and pS235), 'outside' the binding site, could not be ascribed to the formation of the transient α-helical motif.

Upon phosphorylation, an increase in compactness of the Tau peptide was observed, favored by decreasing the temperature for the C36m simulation that best captured the experimental parameters with respect to the A99 simulation. The predictive capacity of generated structural ensembles for the C36m force-field driven simulations encouraged a more detailed structural analysis. This analysis revealed that the phosphorylation is causing multiple contacts between residues, as validated by the observed NOEs signals (**Figures S4 and 7a, Tables S2-3**). The phospho-Tau peptide favored a bent conformation stabilized by these multiple intra-molecular contacts mostly originating from the phosphorylated residues (T217, T231, S235) forming salt bridges with nearby lysine and arginine residues as well as long-range salt-bridges (pT217-R230 and pS235-R221) (**Figure 7B**). In agreement, a previous MD study of a phosphorylated Tau 225-250 peptide, that overlaps with the peptide from the present study and contains pT231 and pS235, also showed formation of salt-bridges that stabilize conformation preferences.[57] Salt bridges were observed with pT231 and pS235, preferentially with the i-1 residue (R230-pT231, K234-pS235) but also with more distant residues (pT231-K240, pT231 /pS235-R242).[57] Similarly, study of Tau peptide 225-246 with 2 or 4 phosphorylations (T231/S235 or T231/S235/S237/S238) showed the formation of a network of salt bridges using NMR parameters and computation of molecular ensembles. pT231 and pS235 favor salt bridges with their directly preceding residues R230 and K234 while pS237 and pS238 are forming salt bridges with distant K240 and R242, respectively.[18] It was proposed that pT231 alone is not sufficient to stabilize the α-helix in Tau(225-246) and while an helix is detected in the NMR spectra for the doubly phosphorylated (pT231-pS235) Tau(225-246), the helical conformation is much increased in the tetra-phosphorylated

(pT231/pS235/pS237/pS238) Tau(225-246) peptide, due to the presence of multiple salt-bridges.[14] In agreement, MD simulations of a Tau(225-245) peptides with 0, 1 or 2 phosphorylations at position T231 and S235 also show that pS235 is not sufficient to affect the conformation of the peptide.[57] A single pT231 or pS235 might thus not be enough to establish the network of salt-bridges that could be necessary to stabilize secondary structures and peptide compaction and consequently, binding affinities of the corresponding peptides (**Figure 1A**). The conformational changes leading to the more compact conformation may indeed be subtly regulating the binding of Tau with BIN1 protein by affecting the accessibility of the binding site. In addition, the intra-molecular salt-bridges involving R221 and K224 in 4P-Tau(210-240) might also impact the binding by competing with intermolecular salt-bridges (**Figure 1D**). We previously showed that mutation of K224 and K225 reduced the affinity for BIN1 SH3 to a Kd of 429 ± 94μM,[22] comparable to the one of 4P-Tau(210-240). It was similarly proposed that pT231 salt bridge to R230 competes with the formation of an intermolecular salt bridge with the microtubules.[14]

These data emphasize the complex regulation of IDPs by multiple phosphorylation, and the importance to consider their combinations and indirect structural effects to further understand their regulatory role in modulating binding with protein partners.

PROTEIN ACCESSION ID

Tau protein, microtubule-associated protein tau isoform 2 [Homo sapiens], 441 amino-acid residues, NCBI reference number NP_005901.2

BIN1 protein, myc box-dependent-interacting protein 1 isoform 1 [Homo sapiens], 593 amino-acid residues, NCBI reference number NP_647593

ASSOCIATED CONTENT

Supporting Information.

Figure S1. Analytical characterization of recombinant 4P-Tau(210-240)
Figure S2 BIN1 SH3 NMR-monitored titration with Tau peptides.
Figure S3 The Tau peptides sample the same bound conformation
Figure S4 NOE contact maps
Figure S5 Comparison of experimental and simulated 3JHA-Hα couplings
Figure S6. Comparison of experimental and simulated secondary chemical shifts
Figure S7. Secondary structure propensity calculated from MD trajectories
Table S1 NOE contact list for Tau(210–240) peptide
Table S2 NOE contact list for 4P-Tau(210–240) peptide
Table S3 Simulated Tau(210–240) peptide ensembles
Table S4 Average radius of gyration calculated from the MD trajectories
Table S3 Occupancy of salt bridges formed during the MD simulations

AUTHOR INFORMATION

Corresponding Authors

* Dr I. Landrieu, Campus CNRS de la Haute Borne – Bâtiment IRI-RMN, 50 avenue de Halley, 59658 Villeneuve d'Ascq, France isabelle.landrieu@univ-lille.fr +33362531712; Dr J. Hritz Office C04/224 Kamenice 753/5, Brno, 625 00, Czech Republic jozef.hritz@ceitec.muni.cz +420 54949 3847

Present Address

† Zernike Institute for Advanced Materials, University of Groningen, Nijenborgh 4, 9747 AG, Groningen, the Netherlands.

Equal contributions

Alessia Lasorsa, Krishnendu Bera and Idir Malki.

Orcid

Alessia Lasorsa: https://orcid.org/0000-0001-6793-5845

Krishnendu Bera: https://orcid.org/0000-0001-9966-5907

Elian Dupré: https://orcid.org/0000-0001-5281-0337

François-Xavier Cantrelle: https://orcid.org/0000-0002-3413-5443

Davy Sinnaeve: https://orcid.org/0000-0003-2556-5895

Xavier Hanoulle: https://orcid.org/0000-0002-3755-2680

Jozef Hritz : https://orcid.org/0000-0002-4512-9241

Isabelle Landrieu: https://orcid.org/0000-0002-4883-2637

Author contributions

Alessia Lasorsa: investigation; methodology; formal analysis; visualization; writing the original draft. Krishnendu Bera: investigation; formal analysis; visualization; writing the original draft. Idir Malki: investigation; methodology; formal analysis; writing-review and editing. Elian Dupré: methodology; supervision; validation; visualization; writing-review and editing. François-Xavier Cantrelle: investigation; methodology; formal analysis. Hamida Merzougui: investigation. Davy

Sinnaeve: validation; writing-review and editing. Xavier Hanoulle: methodology; supervision; validation; writing-review and editing. Jozef Hritz: formal analysis; supervision; validation; writing the original draft; writing-review and editing; conceptualization; funding acquisition. Isabelle Landrieu: formal analysis; methodology; supervision; validation; visualization; writing the original draft; writing-review and editing; conceptualization; funding acquisition.

Funding sources

The 600 MHz NMR facilities were funded by the Nord Region Council, CNRS, Institut Pasteur de Lille, the European Union with the European Regional Development Fund (ERDF), the French Ministry of Research and the University of Lille and by the CTRL CPER co-funded by the European Union (ERDF), by the Hauts de France Regional Council (contrat #17003781), Métropole Européenne de Lille (contract #2016_ESR_05) and French State (contract #2017-R3-CTRL-Phase 1). Financial support from the IR INFRANALYTICS FR2054 for conducting the research is gratefully acknowledged. Computational resources were supplied by the metacentrum and IT4 Innovations National Supercomputing Center (OPEN-17-7), project (e-INFRA CZ 90140 and LM2018140) provided within the program Projects of Large Research, Development and Innovations Infrastructures. This study was supported by the French government funding agency Agence Nationale de la Recherche : LabEx (Laboratory of Excellence) DISTALZ (Development of Innovative Strategies for a Transdisciplinary approach to Alzheimer's disease) and ANR-15-CE16-0002 BinAlz. KB and JH were funded by the Ministry of Education, Youth, and Sport of the Czech Republic (MEYS CR), grant number LTAUSA18168 (Inter-Excellence Inter-Action) and Czech Science Foundation [GF20-05789L]. KB is also supported by Brno Ph.D. Talent Scholarship – funded by the Brno City Municipality, Brno, Czech Republic.

Notes

The authors declare the submitted work was carried out without the presence of any personal, professional or financial relationships that could potentially be construed as a conflict of interest.

ABBREVIATIONS

A99 force field, Amber99SB-ILDN force field; AD, Alzheimer's disease; BIN1, bridging integrator-1 protein; C36m force field, CHARMM36m force field; hetNOE, heteronuclear nuclear overhauser effect; HSQC, heteronuclear single quantum correlation; IDP, intrinsically disordered protein; Kd, dissociation constant; NMR, nuclear magnetic resonance; MD, molecular dynamics; Rg, radius of gyration; pT, phosphothreonine amino-acid residue; PTMs, post-translational modifications; pS, phosphoserine amino-acid residue; RMSD, root mean square deviation; SSP, secondary structure propensity

REFERENCES

(1) Xie, H.; Vucetic, S.; Iakoucheva, L. M.; Oldfield, C. J.; Dunker, A. K.; Obradovic, Z.; Uversky, V. N. Functional Anthology of Intrinsic Disorder. 3. Ligands, Post-Translational Modifications, and Diseases Associated with Intrinsically Disordered Proteins. *J Proteome Res* **2007**, *6* (5), 1917–1932. https://doi.org/10.1021/pr060394e.

(2) Babu, M. M.; Kriwacki, R. W.; Pappu, R. V. Structural Biology. Versatility from Protein Disorder. *Science* **2012**, *337* (6101), 1460–1461. https://doi.org/10.1126/science.1228775.

(3) Bah, A.; Forman-Kay, J. D. Modulation of Intrinsically Disordered Protein Function by Post-Translational Modifications. *J Biol Chem* **2016**, *291* (13), 6696–6705. https://doi.org/10.1074/jbc.R115.695056.

(4) Iešmantavičius, V.; Dogan, J.; Jemth, P.; Teilum, K.; Kjaergaard, M. Helical Propensity in an Intrinsically Disordered Protein Accelerates Ligand Binding. *Angew Chem Int Ed Engl* **2014**, *53* (6), 1548–1551. https://doi.org/10.1002/anie.201307712.

(5) Borcherds, W.; Theillet, F.-X.; Katzer, A.; Finzel, A.; Mishall, K. M.; Powell, A. T.; Wu, H.; Manieri, W.; Dieterich, C.; Selenko, P.; Loewer, A.; Daughdrill, G. W. Disorder and Residual Helicity Alter P53-Mdm2 Binding Affinity and Signaling in Cells. *Nat Chem Biol* **2014**, *10* (12), 1000–1002. https://doi.org/10.1038/nchembio.1668.

(6) Bah, A.; Vernon, R. M.; Siddiqui, Z.; Krzeminski, M.; Muhandiram, R.; Zhao, C.; Sonenberg, N.; Kay, L. E.; Forman-Kay, J. D. Folding of an Intrinsically Disordered Protein by Phosphorylation as a Regulatory Switch. *Nature* **2015**, *519* (7541), 106–109. https://doi.org/10.1038/nature13999.

(7) Espinoza-Fonseca, L. M.; Kast, D.; Thomas, D. D. Thermodynamic and Structural Basis of Phosphorylation-Induced Disorder-to-Order Transition in the Regulatory Light Chain of Smooth Muscle Myosin. *J Am Chem Soc* **2008**, *130* (37), 12208–12209. https://doi.org/10.1021/ja803143g.

(8) Mao, A. H.; Crick, S. L.; Vitalis, A.; Chicoine, C. L.; Pappu, R. V. Net Charge per Residue Modulates Conformational Ensembles of Intrinsically Disordered Proteins. *Proc Natl Acad Sci U S A* **2010**, *107* (18), 8183–8188. https://doi.org/10.1073/pnas.0911107107.

(9) Pufall, M. A.; Lee, G. M.; Nelson, M. L.; Kang, H.-S.; Velyvis, A.; Kay, L. E.; McIntosh, L. P.; Graves, B. J. Variable Control of Ets-1 DNA Binding by Multiple Phosphates in an Unstructured Region. *Science* **2005**, *309* (5731), 142–145. https://doi.org/10.1126/science.1111915.

(10) Nash, P.; Tang, X.; Orlicky, S.; Chen, Q.; Gertler, F. B.; Mendenhall, M. D.; Sicheri, F.; Pawson, T.; Tyers, M. Multisite Phosphorylation of a CDK Inhibitor Sets a Threshold for the Onset of DNA Replication. *Nature* **2001**, *414* (6863), 514–521. https://doi.org/10.1038/35107009.

(11) Poudel, S.; Vanderwall, D.; Yuan, Z.-F.; Wu, Z.; Peng, J.; Li, Y. JUMPptm: Integrated Software for Sensitive Identification of Post-Translational Modifications and Its Application in Alzheimer's Disease Study. *Proteomics* **2022**, e2100369. https://doi.org/10.1002/pmic.202100369.

(12) Amniai, L.; Barbier, P.; Sillen, A.; Wieruszeski, J.-M.; Peyrot, V.; Lippens, G.; Landrieu, I. Alzheimer Disease Specific Phosphoepitopes of Tau Interfere with Assembly of Tubulin but Not Binding to Microtubules. *FASEB J* **2009**, *23* (4), 1146–1152. https://doi.org/10.1096/fj.08-121590.

(13) Sibille, N.; Huvent, I.; Fauquant, C.; Verdegem, D.; Amniai, L.; Leroy, A.; Wieruszeski, J.-M.; Lippens, G.; Landrieu, I. Structural Characterization by Nuclear Magnetic Resonance of the Impact of Phosphorylation in the Proline-Rich Region of the Disordered Tau Protein. *Proteins* **2012**, *80* (2), 454–462. https://doi.org/10.1002/prot.23210.

(14) Schwalbe, M.; Kadavath, H.; Biernat, J.; Ozenne, V.; Blackledge, M.; Mandelkow, E.; Zweckstetter, M. Structural Impact of Tau Phosphorylation at Threonine 231. *Structure* **2015**, *23* (8), 1448–1458. https://doi.org/10.1016/j.str.2015.06.002.

(15) Gandhi, N. S.; Landrieu, I.; Byrne, C.; Kukic, P.; Amniai, L.; Cantrelle, F.-X.; Wieruszeski, J.-M.; Mancera, R. L.; Jacquot, Y.; Lippens, G. A Phosphorylation-Induced Turn Defines the Alzheimer's Disease AT8 Antibody Epitope on the Tau Protein. *Angew Chem Int Ed Engl* **2015**, *54* (23), 6819–6823. https://doi.org/10.1002/anie.201501898.

(16) Bibow, S.; Ozenne, V.; Biernat, J.; Blackledge, M.; Mandelkow, E.; Zweckstetter, M. Structural Impact of Proline-Directed Pseudophosphorylation at AT8, AT100, and PHF1 Epitopes on 441-Residue Tau. *J Am Chem Soc* **2011**, *133* (40), 15842–15845. https://doi.org/10.1021/ja205836j.

(17) Jeganathan, S.; von Bergen, M.; Brutlach, H.; Steinhoff, H.-J.; Mandelkow, E. Global Hairpin Folding of Tau in Solution. *Biochemistry* **2006**, *45* (7), 2283–2293. https://doi.org/10.1021/bi0521543.

(18) Mukrasch, M. D.; Bibow, S.; Korukottu, J.; Jeganathan, S.; Biernat, J.; Griesinger, C.; Mandelkow, E.; Zweckstetter, M. Structural Polymorphism of 441-Residue Tau at Single Residue Resolution. *PLoS Biol* **2009**, *7* (2), e34. https://doi.org/10.1371/journal.pbio.1000034.

(19) Chapuis, J.; Hansmannel, F.; Gistelinck, M.; Mounier, A.; Van Cauwenberghe, C.; Kolen, K. V.; Geller, F.; Sottejeau, Y.; Harold, D.; Dourlen, P.; Grenier-Boley, B.; Kamatani, Y.; Delepine, B.; Demiautte, F.; Zelenika, D.; Zommer, N.; Hamdane, M.; Bellenguez, C.; Dartigues, J.-F.; Hauw, J.-J.; Letronne, F.; Ayral, A.-M.; Sleegers, K.; Schellens, A.; Broeck, L. V.; Engelborghs, S.; De Deyn, P. P.; Vandenberghe, R.; O'Donovan, M.; Owen, M.; Epelbaum, J.; Mercken, M.; Karran, E.; Bantscheff, M.; Drewes, G.; Joberty, G.; Campion, D.; Octave, J.-N.; Berr, C.; Lathrop, M.; Callaerts, P.; Mann, D.; Williams, J.; Buée, L.; Dewachter, I.; Van Broeckhoven, C.; Amouyel, P.; Moechars, D.; Dermaut, B.; Lambert, J.-C.; GERAD consortium. Increased Expression of BIN1 Mediates Alzheimer Genetic Risk by Modulating Tau Pathology. *Mol Psychiatry* **2013**, *18* (11), 1225–1234. https://doi.org/10.1038/mp.2013.1.

(20) Sottejeau, Y.; Bretteville, A.; Cantrelle, F.-X.; Malmanche, N.; Demiaute, F.; Mendes, T.; Delay, C.; Alves Dos Alves, H.; Flaig, A.; Davies, P.; Dourlen, P.; Dermaut, B.; Laporte, J.; Amouyel, P.; Lippens, G.; Chapuis, J.; Landrieu, I.; Lambert, J.-C. Tau Phosphorylation Regulates the Interaction between BIN1's SH3 Domain and Tau's Proline-Rich Domain. *Acta Neuropathol Commun* **2015**, *3*, 58. https://doi.org/10.1186/s40478-015-0237-8.

(21) Malki, I.; Cantrelle, F.-X.; Sottejeau, Y.; Lippens, G.; Lambert, J.-C.; Landrieu, I. Regulation of the Interaction between the Neuronal BIN1 Isoform 1 and Tau Proteins - Role of the SH3 Domain. *FEBS J* **2017**, *284* (19), 3218–3229. https://doi.org/10.1111/febs.14185.

(22) Lasorsa, A.; Malki, I.; Cantrelle, F.-X.; Merzougui, H.; Boll, E.; Lambert, J.-C.; Landrieu, I. Structural Basis of Tau Interaction With BIN1 and Regulation by Tau Phosphorylation. *Front Mol Neurosci* **2018**, *11*, 421. https://doi.org/10.3389/fnmol.2018.00421.

(23) Welburn, J. P. I.; Endicott, J. A. Inhibition of the Cell Cycle with Chemical Inhibitors: A Targeted Approach. *Semin Cell Dev Biol* **2005**, *16* (3), 369–381. https://doi.org/10.1016/j.semcdb.2005.02.008.

(24) Vranken, W. F.; Boucher, W.; Stevens, T. J.; Fogh, R. H.; Pajon, A.; Llinas, M.; Ulrich, E. L.; Markley, J. L.; Ionides, J.; Laue, E. D. The CCPN Data Model for NMR Spectroscopy: Development of a Software Pipeline. *Proteins* **2005**, *59* (4), 687–696. https://doi.org/10.1002/prot.20449.

(25) Delaglio, F.; Grzesiek, S.; Vuister, G. W.; Zhu, G.; Pfeifer, J.; Bax, A. NMRPipe: A Multidimensional Spectral Processing System Based on UNIX Pipes. *J Biomol NMR* **1995**, *6* (3), 277–293. https://doi.org/10.1007/BF00197809.

(26) Camilloni, C.; De Simone, A.; Vranken, W. F.; Vendruscolo, M. Determination of Secondary Structure Populations in Disordered States of Proteins Using Nuclear Magnetic Resonance Chemical Shifts. *Biochemistry* **2012**, *51* (11), 2224–2231. https://doi.org/10.1021/bi3001825.

(27) Tamiola, K.; Acar, B.; Mulder, F. A. A. Sequence-Specific Random Coil Chemical Shifts of Intrinsically Disordered Proteins. *J Am Chem Soc* **2010**, *132* (51), 18000–18003. https://doi.org/10.1021/ja105656t.

(28) Bienkiewicz, E. A.; Lumb, K. J. Random-Coil Chemical Shifts of Phosphorylated Amino Acids. *J Biomol NMR* **1999**, *15* (3), 203–206. https://doi.org/10.1023/a:1008375029746.

(29) Wishart, D. S.; Nip, A. M. Protein Chemical Shift Analysis: A Practical Guide. *Biochem Cell Biol* **1998**, *76* (2–3), 153–163. https://doi.org/10.1139/bcb-76-2-3-153.

(30) Garrett, D. S.; Seok, Y. J.; Liao, D. I.; Peterkofsky, A.; Gronenborn, A. M.; Clore, G. M. Solution Structure of the 30 KDa N-Terminal Domain of Enzyme I of the Escherichia Coli Phosphoenolpyruvate:Sugar Phosphotransferase System by Multidimensional NMR. *Biochemistry* **1997**, *36* (9), 2517–2530. https://doi.org/10.1021/bi962924y.

(31) Warnecke, A.; Sandalova, T.; Achour, A.; Harris, R. A. PyTMs: A Useful PyMOL Plugin for Modeling Common Post-Translational Modifications. *BMC Bioinformatics* **2014**, *15* (1), 370. https://doi.org/10.1186/s12859-014-0370-6.

(32) The PyMOL Molecular Graphics System.

(33) Berendsen, H. J. C.; van der Spoel, D.; van Drunen, R. GROMACS: A Message-Passing Parallel Molecular Dynamics Implementation. *Computer Physics Communications* **1995**, *91* (1), 43–56. https://doi.org/10.1016/0010-4655(95)00042-E.

(34) Lindorff-Larsen, K.; Piana, S.; Palmo, K.; Maragakis, P.; Klepeis, J. L.; Dror, R. O.; Shaw, D. E. Improved Side-Chain Torsion Potentials for the Amber Ff99SB Protein Force Field. *Proteins: Structure, Function, and Bioinformatics* **2010**, *78* (8), 1950–1958. https://doi.org/10.1002/prot.22711.

(35) Huang, J.; Rauscher, S.; Nawrocki, G.; Ran, T.; Feig, M.; de Groot, B. L.; Grubmüller, H.; MacKerell, A. D. CHARMM36m: An Improved Force Field for Folded and Intrinsically Disordered Proteins. *Nature Methods* **2017**, *14* (1), 71–73. https://doi.org/10.1038/nmeth.4067.

(36) Piana, S.; Donchev, A. G.; Robustelli, P.; Shaw, D. E. Water Dispersion Interactions Strongly Influence Simulated Structural Properties of Disordered Protein States. *J. Phys. Chem. B* **2015**, *119* (16), 5113–5123. https://doi.org/10.1021/jp508971m.

(37) Zapletal, V.; Mládek, A.; Melková, K.; Louša, P.; Nomilner, E.; Jaseňáková, Z.; Kubáň, V.; Makovická, M.; Laníková, A.; Žídek, L.; Hritz, J. Choice of Force Field for Proteins Containing Structured and Intrinsically Disordered Regions. *Biophysical Journal* **2020**, *118* (7), 1621–1633. https://doi.org/10.1016/j.bpj.2020.02.019.

(38) Hess, B.; Bekker, H.; Berendsen, H. J. C.; Fraaije, J. G. E. M. LINCS: A Linear Constraint Solver for Molecular Simulations. *Journal of Computational Chemistry* **1997**, *18* (12), 1463–1472. https://doi.org/10.1002/(SICI)1096-987X(199709)18:12<1463::AID-JCC4>3.0.CO;2-H.

(39) Essmann, U.; Perera, L.; Berkowitz, M. L.; Darden, T.; Lee, H.; Pedersen, L. G. A Smooth Particle Mesh Ewald Method. *The Journal of Chemical Physics* **1995**, *103* (19), 8577–8593. https://doi.org/10.1063/1.470117.

(40) Bussi, G.; Donadio, D.; Parrinello, M. Canonical Sampling through Velocity Rescaling. *The Journal of Chemical Physics* **2007**, *126* (1), 014101. https://doi.org/10.1063/1.2408420.

(41) Parrinello, M.; Rahman, A. Polymorphic Transitions in Single Crystals: A New Molecular Dynamics Method. *Journal of Applied Physics* **1981**, *52* (12), 7182–7190. https://doi.org/10.1063/1.328693.

(42) Bera, K. Binding and Inhibitory Effect of Ravidasvir on 3CL ^{pro} of SARS-CoV-2: A Molecular Docking, Molecular Dynamics and MM/PBSA Approach. *Journal of Biomolecular Structure and Dynamics* **2021**, 1–8. https://doi.org/10.1080/07391102.2021.1896388.

(43) Han, B.; Liu, Y.; Ginzinger, S. W.; Wishart, D. S. SHIFTX2: Significantly Improved Protein Chemical Shift Prediction. *J Biomol NMR* **2011**, *50* (1), 43–57. https://doi.org/10.1007/s10858-011-9478-4.

(44) Mercadante, D.; Gräter, F.; Daday, C. CONAN: A Tool to Decode Dynamical Information from Molecular Interaction Maps. *Biophysical Journal* **2018**, *114* (6), 1267–1273. https://doi.org/10.1016/j.bpj.2018.01.033.

(45) Wright, P. E.; Dyson, H. J. Intrinsically Disordered Proteins in Cellular Signalling and Regulation. *Nat Rev Mol Cell Biol* **2015**, *16* (1), 18–29. https://doi.org/10.1038/nrm3920.

(46) Brister, M. A.; Pandey, A. K.; Bielska, A. A.; Zondlo, N. J. OGlcNAcylation and Phosphorylation Have Opposing Structural Effects in Tau: Phosphothreonine Induces Particular Conformational Order. *J Am Chem Soc* **2014**, *136* (10), 3803–3816. https://doi.org/10.1021/ja407156m.

(47) Kim, S.-Y.; Jung, Y.; Hwang, G.-S.; Han, H.; Cho, M. Phosphorylation Alters Backbone Conformational Preferences of Serine and Threonine Peptides. *Proteins* **2011**, *79* (11), 3155–3165. https://doi.org/10.1002/prot.23148.

(48) Delaforge, E.; Milles, S.; Huang, J.-R.; Bouvier, D.; Jensen, M. R.; Sattler, M.; Hart, D. J.; Blackledge, M. Investigating the Role of Large-Scale Domain Dynamics in Protein-Protein Interactions. *Front Mol Biosci* **2016**, *3*, 54. https://doi.org/10.3389/fmolb.2016.00054.

(49) Joosten, R. P.; te Beek, T. A. H.; Krieger, E.; Hekkelman, M. L.; Hooft, R. W. W.; Schneider, R.; Sander, C.; Vriend, G. A Series of PDB Related Databases for Everyday Needs. *Nucleic Acids Research* **2011**, *39* (Database), D411–D419. https://doi.org/10.1093/nar/gkq1105.

(50) Kabsch, W.; Sander, C. Dictionary of Protein Secondary Structure: Pattern Recognition of Hydrogen-Bonded and Geometrical Features. *Biopolymers* **1983**, *22* (12), 2577–2637. https://doi.org/10.1002/bip.360221211.

(51) Sheinerman, F. B.; Honig, B. On the Role of Electrostatic Interactions in the Design of Protein-Protein Interfaces. *J Mol Biol* **2002**, *318* (1), 161–177. https://doi.org/10.1016/S0022-2836(02)00030-X.

(52) Selzer, T.; Albeck, S.; Schreiber, G. Rational Design of Faster Associating and Tighter Binding Protein Complexes. *Nat Struct Biol* **2000**, *7* (7), 537–541. https://doi.org/10.1038/76744.

(53) Wu, D.; Zhou, H.-X. Designed Mutations Alter the Binding Pathways of an Intrinsically Disordered Protein. *Sci Rep* **2019**, *9* (1), 6172. https://doi.org/10.1038/s41598-019-42717-6.

(54) Sherry, K. P.; Das, R. K.; Pappu, R. V.; Barrick, D. Control of Transcriptional Activity by Design of Charge Patterning in the Intrinsically Disordered RAM Region of the Notch Receptor. *Proc Natl Acad Sci U S A* **2017**, *114* (44), E9243–E9252. https://doi.org/10.1073/pnas.1706083114.

(55) Sinnaeve, D.; Ben Bouzayene, A.; Ottoy, E.; Hofman, G.-J.; Erdmann, E.; Linclau, B.; Kuprov, I.; Martins, J. C.; Torbeev, V.; Kieffer, B. Fluorine NMR Study of Proline-Rich Sequences Using Fluoroprolines. *Magnetic Resonance* **2021**, *2* (2), 795–813. https://doi.org/10.5194/mr-2-795-2021.

(56) Bielska, A. A.; Zondlo, N. J. Hyperphosphorylation of Tau Induces Local Polyproline II Helix. *Biochemistry* **2006**, *45* (17), 5527–5537. https://doi.org/10.1021/bi052662c.

(57) Lyons, A. J.; Gandhi, N. S.; Mancera, R. L. Molecular Dynamics Simulation of the Phosphorylation-Induced Conformational Changes of a Tau Peptide Fragment. *Proteins* **2014**, *82* (9), 1907–1923. https://doi.org/10.1002/prot.24544.

(58) Boehr, D. D.; Nussinov, R.; Wright, P. E. The Role of Dynamic Conformational Ensembles in Biomolecular Recognition. *Nat Chem Biol* **2009**, *5* (11), 789–796. https://doi.org/10.1038/nchembio.232.

(59) Fuxreiter, M.; Simon, I.; Friedrich, P.; Tompa, P. Preformed Structural Elements Feature in Partner Recognition by Intrinsically Unstructured Proteins. *J Mol Biol* **2004**, *338* (5), 1015–1026. https://doi.org/10.1016/j.jmb.2004.03.017.

For Table of Contents Only

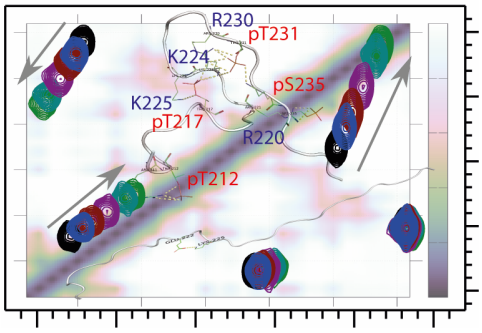

Supplementary Information

Conformation and affinity modulations by multiple phosphorylation occurring in the BIN1 SH3 domain binding site of Tau protein proline-rich region

Alessia Lasorsa[1,2 †#], Krishnendu Bera[3, 4, 5#], Idir Malki1[#], Elian Dupré[1,2], François-Xavier Cantrelle[1,2], Hamida Merzougui[1], Davy Sinnaeve[1,2], Xavier Hanoulle[1,2], Jozef Hritz[3, 5] and Isabelle Landrieu[1,2*]*

[1]CNRS EMR9002 Integrative Structural Biology, F-59000, Lille, France

[2]Univ. Lille, Inserm, CHU Lille, Institut Pasteur de Lille, U1167 - RID-AGE - Risk Factors and Molecular Determinants of Aging-Related Diseases, F-59000, Lille, France

[3]CEITEC MU, Masaryk University, Kamenice 753/5, 625 00 Brno, Czech Republic

[4]National Centre for Biomolecular Research, Faculty of Science, Masaryk University, Kamenice 5, 625 00, Brno, Czech Republic

[5]Department of Chemistry, Faculty of Science, Masaryk University, Kamenice 5, 625 00 Brno, Czech Republic

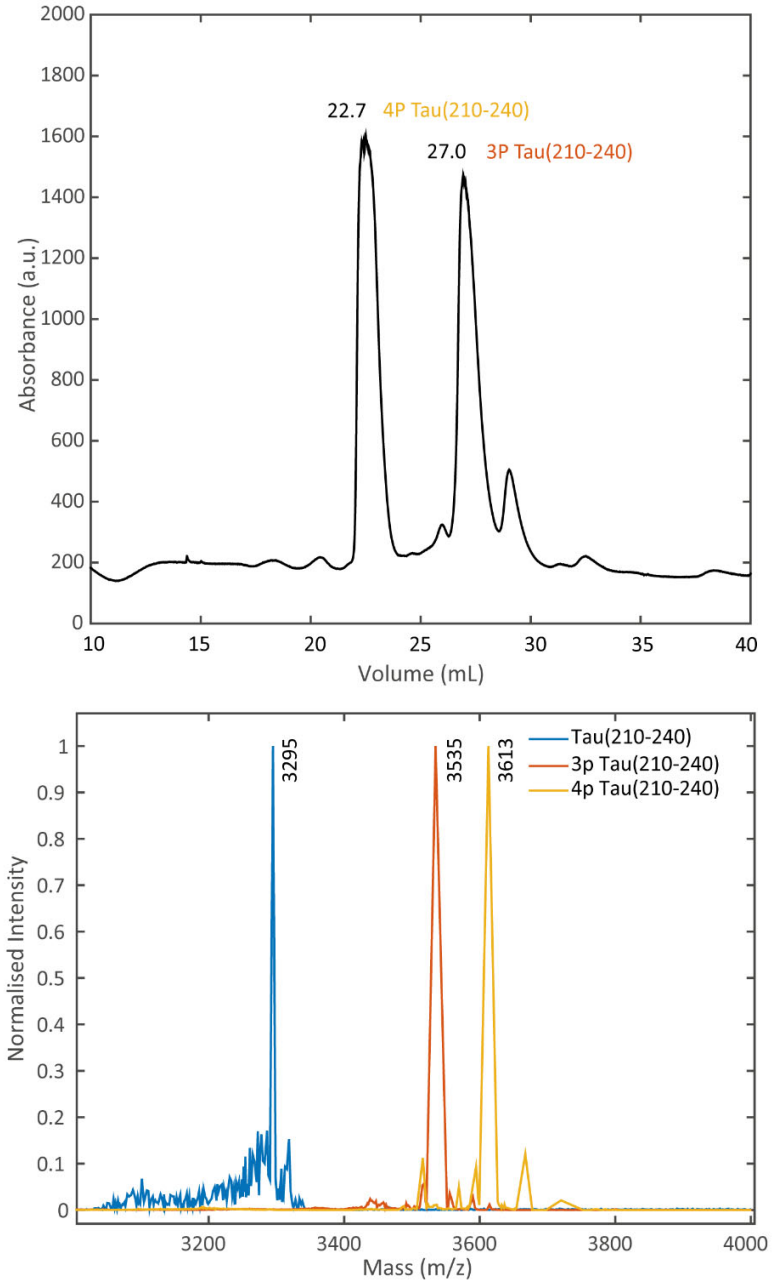

Figure S1. Ion exchange chromatogram of the phosphorylated peptides eluting at different retention volumes, with the related mass spectra. The elution volume shifts from 22.7 to 27.0 mL for the 4P- and the 3P-Tau(210-240) peptides.

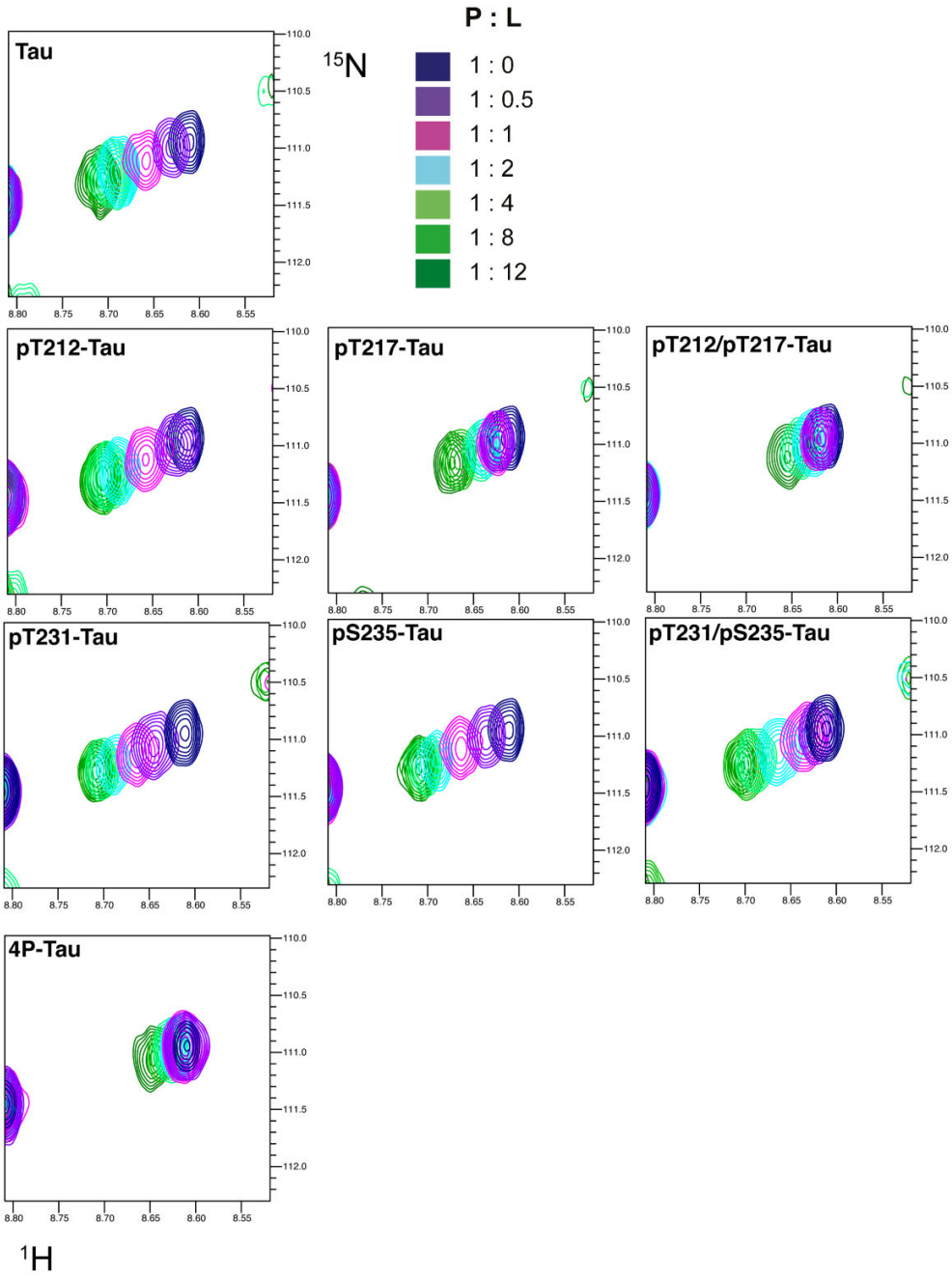

Figure S2. Superposition of ^{1}H,^{15}N HSQC spectra of BIN1 SH3 zoomed around T589 resonance in the presence of increasing amounts of different phosphorylated Tau(210–240) peptides (from blue to green).

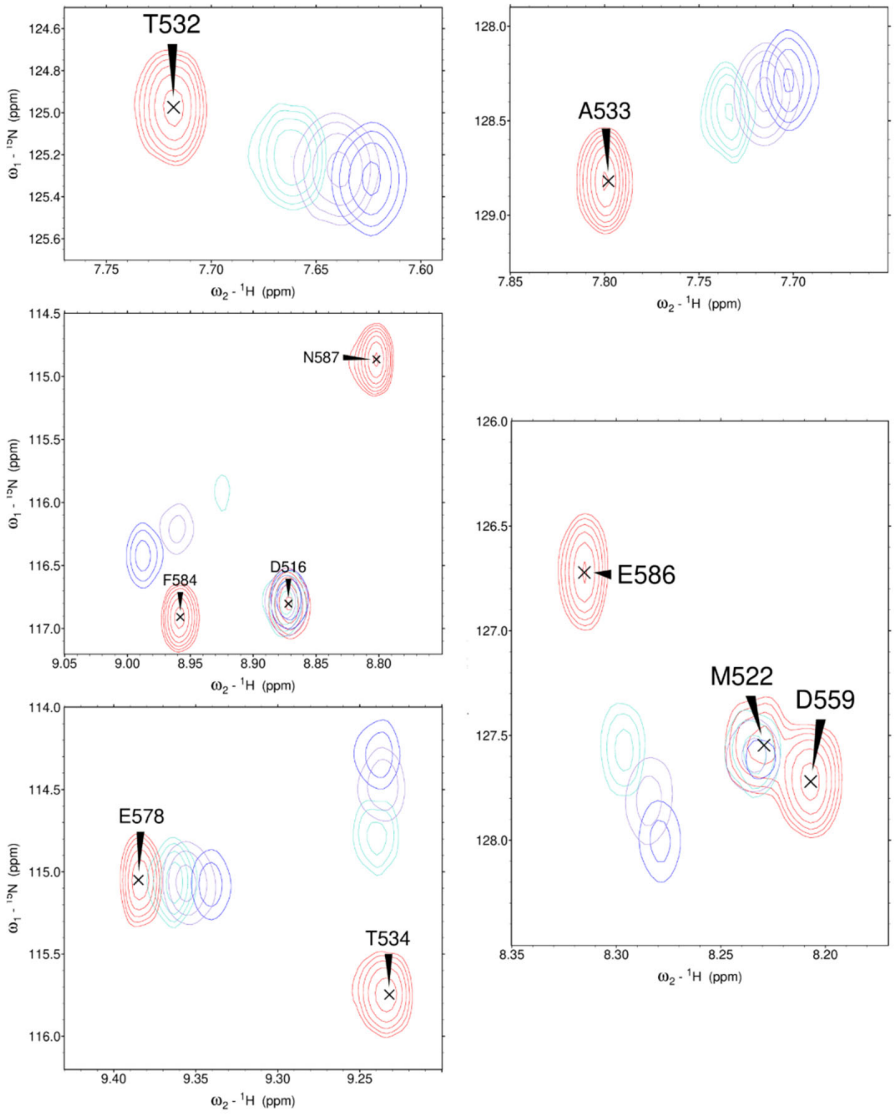

Figure S3. Superposition of enlarged regions of the $^{1}H,^{15}N$ HSQC spectra of BIN1 SH3, free in solution (red) or in the presence of a four-fold excess of Tau(210–240) peptide (blue), 2P-Tau(210–240) peptide (purple) and 4P-Tau(210–240) peptide (green). The observed "diagonal" (or straight line) formed by the corresponding resonances in each of these spectra between the resonance of the free (red resonance) and bound (blue resonance) states show that the phosphorylated peptides sample the same bound conformation as the Tau(210–240) peptide and that only the proportion of complex presents in the solution is modified at a given stoichiometry (here 1 SH3 BIN: 4 Tau(210-240) peptide).

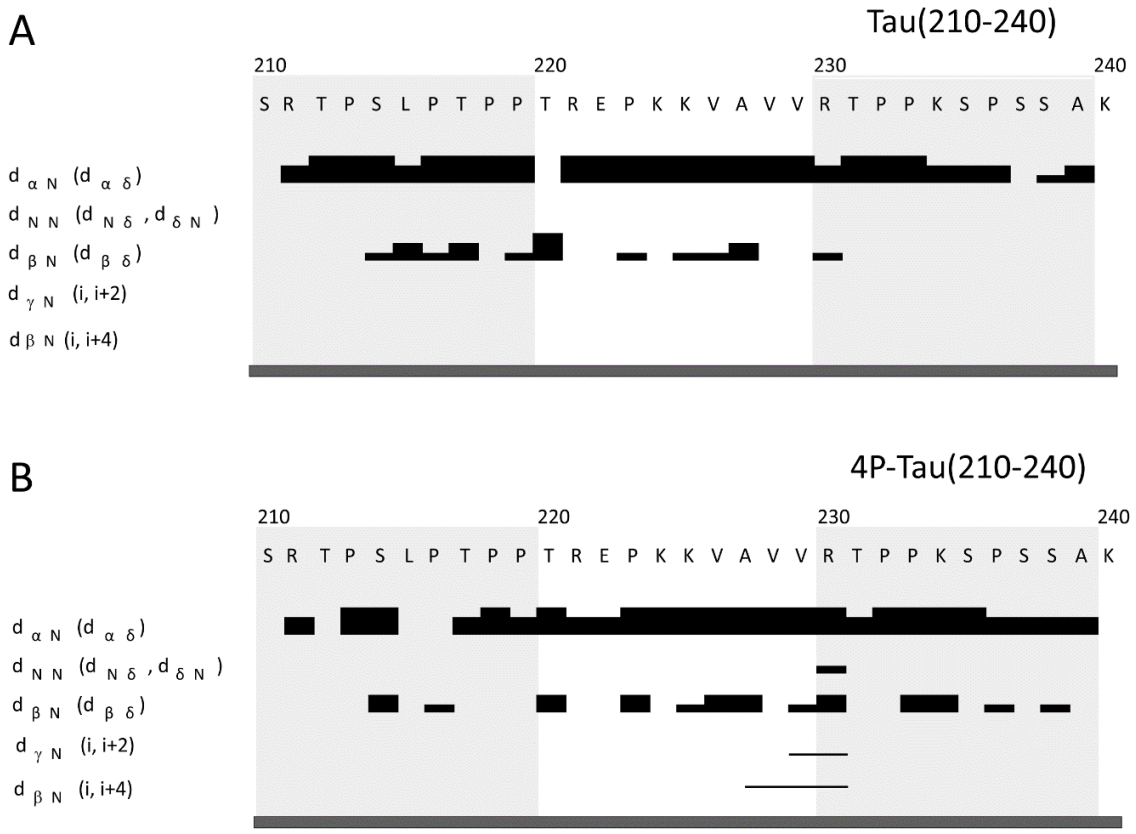

Figure S4. Schematic representation of NOE contacts derived from 3D ^{15}N and ^{13}C HSQC NOESY spectra of A. Tau(210-240) peptide and B. 4P-Tau(210-240) peptide.

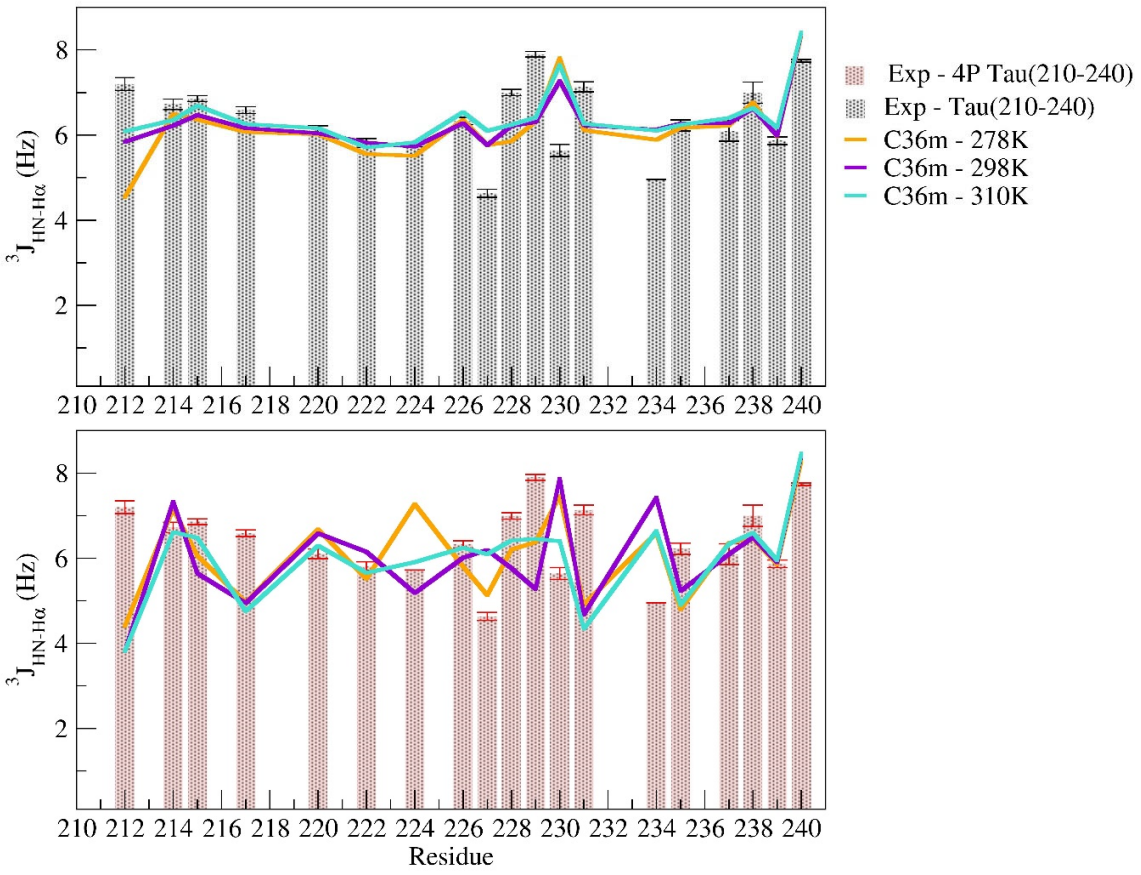

Figure S5. Residue-specific differences in $^3J_{HN-H\alpha}$ couplings of Tau(210-240) or 4P-Tau(210-240) calculated from MD simulations using the C36m force field or from experimental data.

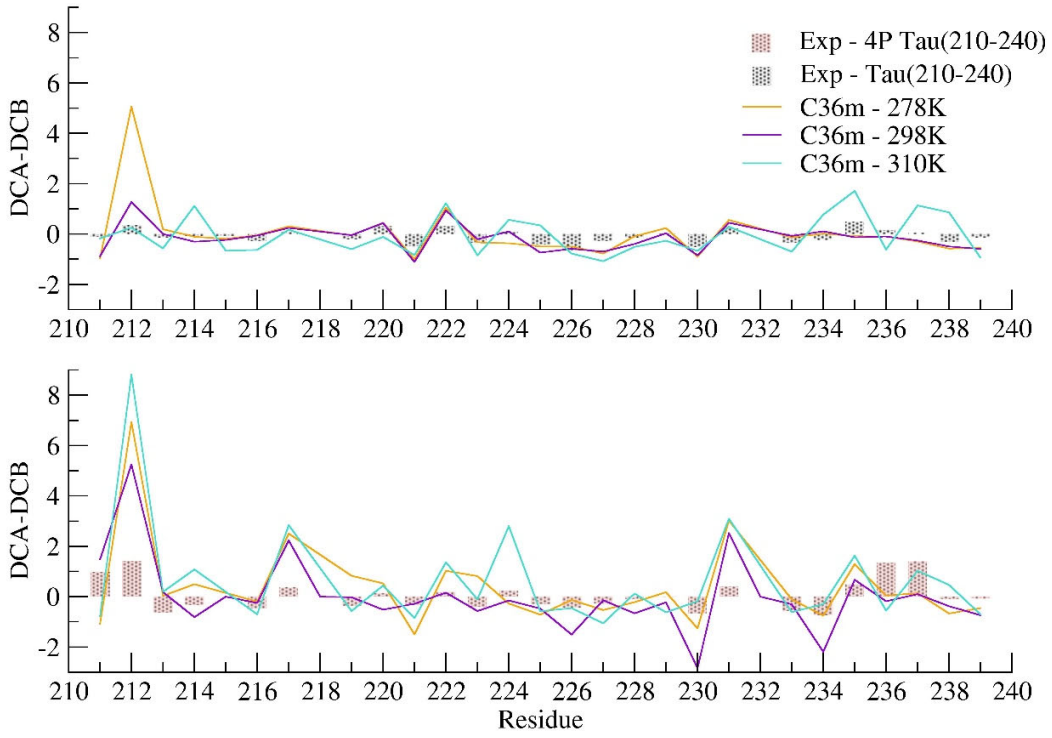

Figure S6. Comparison of experimental and predicted Cα, Cβ secondary chemical shifts differences from C36m MD trajectories.

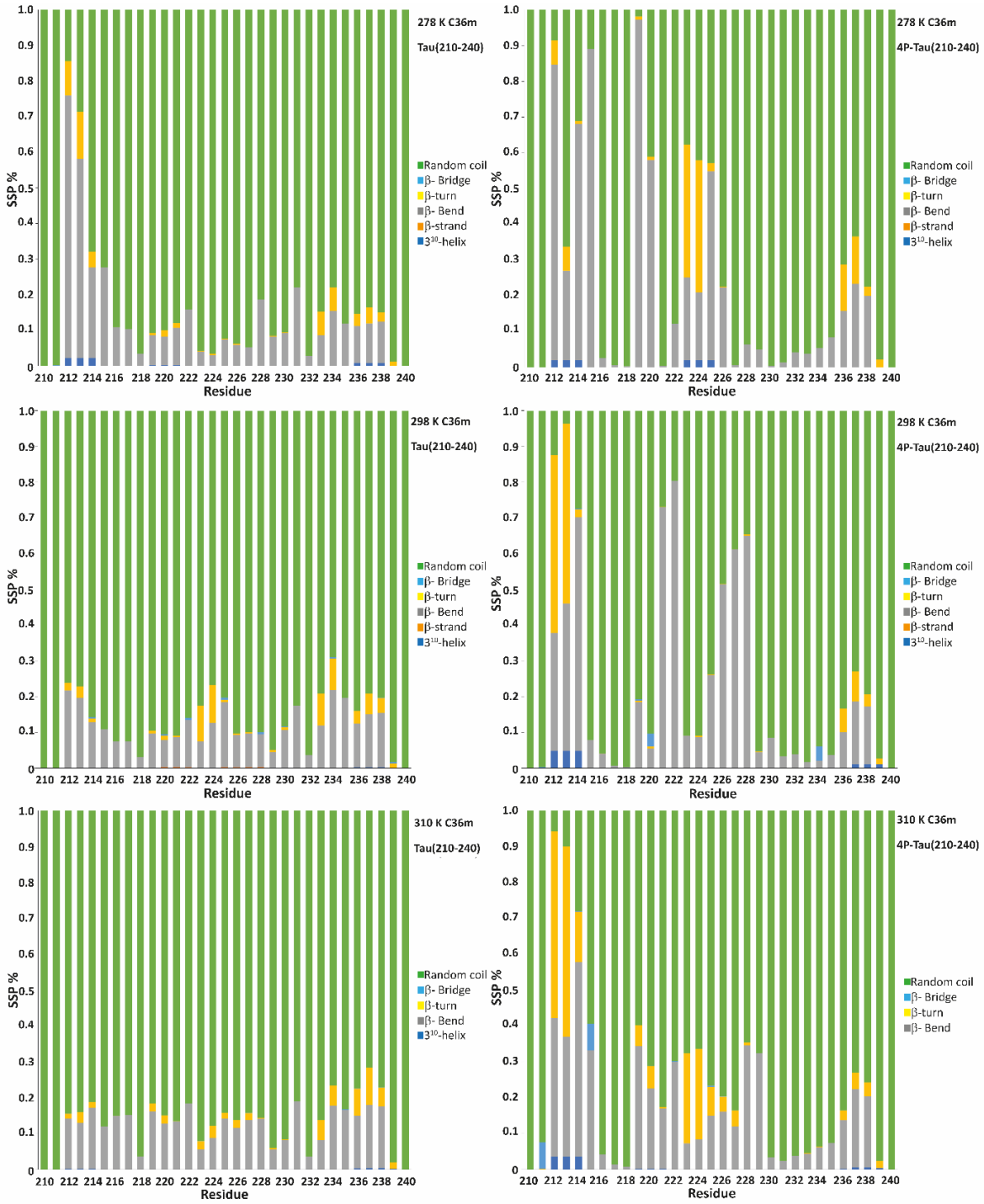

Figure S7. Secondary structure propensity (SSP) calculated from C36m MD trajectories

Supplementary Tables

Table S1. NOE contacts derived from ^{15}N HSQC NOESY recorded on Tau(210–240) peptide.

Assign F1	Assign F2	Assign F3	Volume
212ThrH	212ThrN	211ArgHa	1,92E+12
214SerH	214SerN	213ProHa	5,95E+12
215LeuH	215LeuN	214SerHa	1,05E+13
215LeuH	215LeuN	214SerHb	1,63E+12
217ThrH	217ThrN	216ProHa	1,20E+13
217ThrH	217ThrN	216ProHb	1,23E+12
220ThrH	220ThrN	219ProHa	1,27E+13
220ThrH	220ThrN	219ProHb	1,33E+12
221ArgH	221ArgN	220ThrHb	1,32E+13
222GluH	222GluN	221ArgHa	9,11E+12
224LysH	224LysN	223ProHa	1,26E+13
224LysH	224LysN	223ProHb	1,33E+12
225LysH	225LysN	224LysHa	1,61E+13
226ValH	226ValN	225LysHa	1,74E+13
226ValH	226ValN	225LysHb	2,52E+12
226ValH	226ValN	225LysHd	1,62E+12
227AlaH	227AlaN	226ValHa	1,30E+13
227AlaH	227AlaN	226ValHb	1,32E+12
227AlaH	227AlaN	226ValHg	2,32E+12
228ValH	228ValN	227AlaHa	2,09E+13
228ValH	228ValN	227AlaHb	3,26E+12
229ValH	229ValN	228ValHa	2,07E+13
230ArgH	230ArgN	229ValHa	1,05E+13
230ArgH	230ArgN	229ValHg	2,10E+12
231ThrH	231ThrN	230ArgHa	9,67E+12
231ThrH	231ThrN	230ArgHb	1,47E+12
234LysH	234LysN	233ProHa	1,21E+13
235SerH	235SerN	234LysHa	3,25E+12
239AlaH	239AlaN	238SerHa	2,10E+12
240LysH	240LysN	239AlaHa	3,52E+12

Table S2. NOE contacts derived from ^{15}N HSQC NOESY recorded on 4P-Tau(210–240) peptide. Non-sequential NOEs are highlighted.

Assign F1	Assign F2	Assign F3	Volume
212ThrH	212ThrN	211ArgHa	1,29E+13
215LeuH	215LeuN	214SerHa	2,43E+13
215LeuH	215LeuN	214SerHb	4,70E+12
217ThrH	217ThrN	216Pro(Hb/Hg)	1,58E+12
220ThrH	220ThrN	219ProHa	1,54E+13
220ThrH	220ThrN	219ProHg	2,47E+12
221ArgH	221ArgN	220ThrHa	2,83E+13
221ArgH	221ArgN	220ThrHb	1,78E+13
222GluH	222GluN	221ArgHa	2,07E+13
224LysH	224LysN	223ProHa	3,55E+13
224LysH	224LysN	223ProHb	3,96E+12
225LysH	225LysN	224LysHa	4,19E+13
226ValH	226ValN	225LysHa	3,79E+13
226ValH	226ValN	225LysHb	3,20E+12
226ValH	226ValN	225LysHg	1,81E+12
226ValH	226ValN	225LysHd	4,30E+12
227AlaH	227AlaN	226ValHa	4,00E+13
227AlaH	227AlaN	226ValHb	4,27E+12
227AlaH	227AlaN	226ValHg	6,75E+12
228ValH	228ValN	227AlaHa	4,61E+13
228ValH	228ValN	227AlaHb	7,69E+12
229ValH	229ValN	228ValHa	5,18E+13
230ArgH	230ArgN	231ThrH	2,65E+12
230ArgH	230ArgN	229ValHa	4,02E+13
230ArgH	230ArgN	229ValHb	3,58E+12
230ArgH	230ArgN	229ValHg	8,48E+12
231ThrH	231ThrN	230ArgHa	5,41E+13
231ThrH	231ThrN	230ArgHb	6,47E+12
231ThrH	231ThrN	229ValHg	1,58E+12
231ThrH	231ThrN	227AlaHb	5,19E+12
234LysH	234LysN	233ProHa	4,51E+13
234LysH	234LysN	233ProHb	3,74E+12
235SerH	235SerN	234LysHa	2,51E+13
235SerH	235SerN	234LysHb	5,15E+12
235SerH	235SerN	234LysHg	1,29E+12
235SerH	235SerN	234LysHd	2,82E+12
237SerH	237SerN	236Pro(Hb/Hg)	3,10E+12
239AlaH	239AlaN	238SerHa	8,67E+12
239AlaH	239AlaN	238SerHb	2,27E+12
240LysH	240LysN	239AlaHa	8,42E+12

Table S3. Simulated Tau(210–240) Peptide Ensembles

Sl. No.	System Consists of	Temp (K)	System	Time
1	Amber99sb-ildn (A99) Force Field TIP4PD Water Model 50 mM NaCl Trans Prolines Phos Thr/Ser Charge -2 Cubic Box Capped Terminal NH_3^+ and COO^-	310	Tau(210-240)	1µs
2			4P-Tau(210-240)	1µs
3		298	Tau(210-240)	1µs
4			4P-Tau(210-240)	1µs
5		278	Tau(210-240)	1µs
6			4P-Tau(210-240)	1µs
7	Charmm36m (C36m) Force Field TIP4PD Water Model Trans Prolines 50 mM NaCl Phos Thr/Ser Charge -2 Cubic Box Capped Terminal NH_3^+ and COO^-	310	Tau(210-240)	2µs
8			4P-Tau(210-240)	2µs
9		298	Tau(210-240)	2µs
10			4P-Tau(210-240)	2µs
11		278	Tau(210-240)	2µs
12			4P-Tau(210-240)	2µs

Table S4. Average Radius of Gyration (Rg) calculated from the C36m MD trajectories

Force Field	Temp (K)	System	Average Rg (nm)	Standard Deviations
C36m	310	Tau(210-240)	2.05	0.28
		4P-Tau(210-240)	1.73	0.41
	298	Tau(210-240)	2.06	0.32
		4P-Tau(210-240)	1.40	0.43
	278	Tau(210-240)	2.1	0.26
		4P-Tau(210-240)	1.48	0.21

Table S5. Occupancy of Salt bridges formed during the MD simulations, with a cut-off set at 0.55 nm between the bond forming atoms.

System	Temp (K)	Salt Bridges	Occupancy (%)
4P-Tau(210-240) C36m	278	217THR (P) – 224LYS (N^{ζ})	16.8
		217THR (P) – 225 LYS (N^{ζ})	0.4
		217THR (P) – 230ARG (C^{ζ})	50.3
		231THR (P) - 230ARG (C^{ζ})	18
		231THR (P) – 234LYS (N^{ζ})	53.4
	298	217THR (P) – 225 LYS (N^{ζ})	8.5
		217THR (P) – 234LYS (N^{ζ})	0.9
		217THR (P) – 230ARG (C^{ζ})	51.8
		217THR (P) – 224LYS (N^{ζ})	66.7
		231THR (P) - 224LYS (N^{ζ})	22.2
		231THR (P) – 234LYS (N^{ζ})	78.4
		231THR (P) - 230ARG (C^{ζ})	93
		235SER (P) – 221ARG (C^{ζ})	61.4
	310	217THR (P) – 221ARG (C^{ζ})	49.7
		217THR (P) – 225 LYS (N^{ζ})	0.9
		217THR (P) – 234LYS (N^{ζ})	1.9
		231THR (P) – 230ARG (C^{ζ})	74.2
		231THR (P) – 234LYS (N^{ζ})	34.5
		231THR (P) – 224LYS (N^{ζ})	6.4